THESIS FOR THE DEGREE OF LICENTIATE

Narrow-linewidth optical coherent oscillators in ultra-low loss silicon nitride

Yi Sun

CHALMERS

Photonics Laboratory
Department of Microtechnology and Nanoscience (MC2)
Chalmers University of Technology
Göteborg, Sweden, 2025

Narrow-linewidth optical coherent oscillators in ultra-low loss silicon nitride
Yi Sun
Göteborg, January 2025

ISSN 1652-0769
Technical Report MC2-452

Photonics Laboratory
Department of Microtechnology and Nanoscience (MC2)
Chalmers University of Technology
SE–412 96 Göteborg
Sweden
Telephone: +46 (0)31–772 10 00

Printed in Sweden by
Reproservice
Chalmers Tekniska Högskola
Göteborg, Sweden, 2025

Narrow-linewidth optical coherent oscillators in ultra-low loss silicon nitride

Yi Sun
Photonics Laboratory
Department of Microtechnology and Nanoscience (MC2)
Chalmers University of Technology

Abstract

In recent years, advancements in technologies such as optical coherent communication, precision measurement, optical detection and ranging, have raised the bar for the coherence, power, noise, and other key parameters of light sources. On-chip light sources have emerged as the ideal solution when small size, low weight, low power consumption and cost-effectiveness matter the most. Currently, integrated light sources include semiconductor lasers and chip-based optical parametric oscillators. However, due to their small cavity volume, both types suffer from high quantum noise, poor coherence compared to solid-state or gas lasers.

As a popular integrated photonic platform, silicon nitride has a significant potential for addressing these challenges since it has high nonlinearity, wide transparent window, and good compatibility with other materials. In our previous work, we have realized low-loss long waveguides and high-Q microring resonators. In this thesis, we further reduce the propagation loss of dispersion-engineered silicon nitride waveguides by smoothing the sidewall roughness. By periodically modulating the intrinsic and extrinsic Q factors of the microring resonator, we achieve an on-chip optical parametric oscillator with an output power of 215 mW and an intrinsic linewidth of 220 Hz. In addition, we suppress the frequency noise of both semiconductor lasers and soliton microsombs using an original self-injection locking method. We reduce the intrinsic linewidth of the semiconductor laser from 818 000 Hz to 135 Hz, and compress the intrinsic linewidth of comb lines of the soliton microcomb to below 1 Hz. These results pave the way for on-chip integration of high-power, narrow-linewidth lasers and optical parametric oscillators.

Keywords: integrated photonics, silicon nitride, low loss, frequency noise, semiconductor laser, optical parametric oscillator, narrow linewidth

Acknowledgements

First, I would like to express my sincere gratitude to my supervisor, Prof. Victor Torres-Company, for his selfless guidance, valuable advice, continuous support and encouragement throughout my research process. I am also grateful to my co-supervisor Prof. Bart Kuyken, Asst. Prof. Raphaël Van Laer and examiner Prof. Åsa Haglund, for profound academic insights, meticulous advice. I am also thankful to Prof. Peter Andrekson, and Prof. Magnus Karlsson for sharing knowledge and insights.

I would like to express my special thanks to Prof. Fuchuan Lei for patiently teaching experimental techniques, which enabled me to successfully complete the relevant experimental work. His professional knowledge and experimental support played a key role in the smooth progress of my project. At the same time, I would like to thank Dr. Zhichao Ye, Dr. Marcello Girardi, Yan Gao for their guidance in manufacturing photonic devices. Their experience and technical support were of great help to my research.

I am thankful to Carmen Haide López Ortega, Sara Persia, Vijay Shekhawat, Tim Fuhrmann, Niklas Hammerschmidt for creating a harmonious and orderly environment for everyone, allowing us to share research progresses, help each other, and grow together. I also thank Dr. Óskar B. Helgason, Dr. Israel Rebolledo-Salgado, Dr. Krishna Sundar Twayana, for their valuable contributions to the laboratory.

Additionally, I would like to every member of the Photonics laboratory for their invaluable support and collaboration. My heartfelt thanks also go to the personnel responsible for maintaining equipment in the clean room, whose efforts are important to this work.

I would like to express my sincere gratitude to my parents and friends for their unconditional love and support, especially when I encountered difficulties and challenges. Their trust and support have always been my driving force to move forward.

Acronyms

LiDRA	light detection and ranging
DFB	distributed feedback
DBR	distributed Bragg reflector
CMOS	complementary metal–oxide–semiconductor
PIC	photonic integrated circuit
FP	Fabry-Perot
FSR	free spectral range
RIN	relative intensity noise
SIL	self-injection locking
PSD	power spectral density
FWHM	full width at half-maximum
OPO	optical parametric oscillator
AOM	acousto-optic modulator
EDFA	erbium doped fiber amplifier
LPCVD	low-pressure chemical vapor deposition
SEM	scanning electron microscopy

Publications

This thesis is based on the following publications:

[A] **Yi Sun**, Zhichao Ye, Raphaël Van Laer, Anders Larsson, and Victor Torres-Company, "Low-loss dispersion-engineered silicon nitride waveguides coated with a thin blanket layer", *Conference on Lasers and Electro-Optics*, San Jose, USA, paper JW3B.183, 2022.

[B] **Yi Sun**, Fuchuan Lei, Yan Gao, and Victor Torres-Company, "High-power on-chip hyperparametric oscillator", to be submitted, 2024.

[C] Fuchuan Lei, **Yi Sun**, Óskar B. Helgason, Zhichao Ye, Yan Gao, Magnus Karlsson, Peter A. Andrekson, and Victor Torres-Company, "Self-injection-locked optical parametric oscillator based on microcombs", *Optica*, vol. 11, no. 3, pp. 420-426, 2024.

Related publications and conference contributions by the author, not included in the thesis):

[D] Fuchuan Lei, **Yi Sun**, Óskar B. Helgason, Zhichao Ye, Yan Gao, Magnus Karlsson, Peter A. Andrekson, and Victor Torres-Company, "Narrow-linewidth and tunable parametric oscillator", *Conference on Lasers and Electro-Optics*, Charlotte, USA, paper STh3I.3, 2024.

[E] Yan Gao, **Yi Sun**, Israel Rebolledo-Salgado, Raphaël Van Laer, Victor Torres-Company, and Jochen Schröder, "Z-cut, ultralow-loss, tightly-confined lithium niobate long waveguide", submitted, 2025.

Contents

Chapter 1

Introduction

1.1 Historical overview

Since the demonstration of the first laser in 1960 [1], the wavelength range, output power, optical linewidth and other parameters have been continuously improved, promoting the rapid development of information technologies, scientific research, life sciences and other fields [2–6]. In recent years, breakthroughs in technologies such as light detection and ranging (LiDAR) [7], optical clocks [8], optical coherent communications [9] and precision measurement [10] have put forward higher requirements for parameters such as coherence and noise of light sources. Narrow-linewidth light sources have become research hotspots [11–13].

Narrow-linewidth semiconductor lasers

Narrow-linewidth semiconductor lasers are a new generation of ideal light sources due to their small size, light weight, low power consumption and low cost [14–17].

The earliest semiconductor lasers have a single cavity, such as the Fabry–Pérot (FP) cavity [18], which has two reflectors shown in Fig. 1.1(a). The transverse mode of a laser is determined by the lateral size of the laser, while the longitudinal mode is determined by the laser cavity length. Single-cavity lasers can be divided into short-cavity structures and long-cavity structures according to the cavity length. The short-cavity laser structure has a larger longitudinal mode spacing and can achieve single longitudinal mode operation without any assistance or mode selection, but due to the short photon lifetime, the intrinsic linewidth is large [19]. The long-cavity structure has a narrow linewidth

characteristic, but the longitudinal mode spacing is too small, so the technical difficulty of constructing this laser lies in how to achieve single longitudinal mode operation.

In order to improve the stability of the laser system and integrate the wavelength selective device into the laser cavity, a distributed Bragg reflector (DBR) was proposed [20]. The DBR type cavity is designed based on the FP cavity, and a periodic passive Bragg structure is used instead as a mirror to provide wavelength selective optical feedback. The DBR type cavity has certain filtering characteristics due to the periodic perturbation by the Bragg structure. Combined with the large longitudinal mode spacing brought by the short cavity, it is easy to attain a single longitudinal mode.

By combining the Bragg structure with the gain region and adding a phase shift region to the Bragg structure, a distributed feedback (DFB) structure was formed [21]. The DFB structure combines the feedback and amplification parts together, so the structure is more compact and features tighter integration. The introduction of the phase shift region further limits the light field distribution, so that the DFB structure can overcome the defects of wavelength drift and mode hopping of the DBR structure and works more stably.

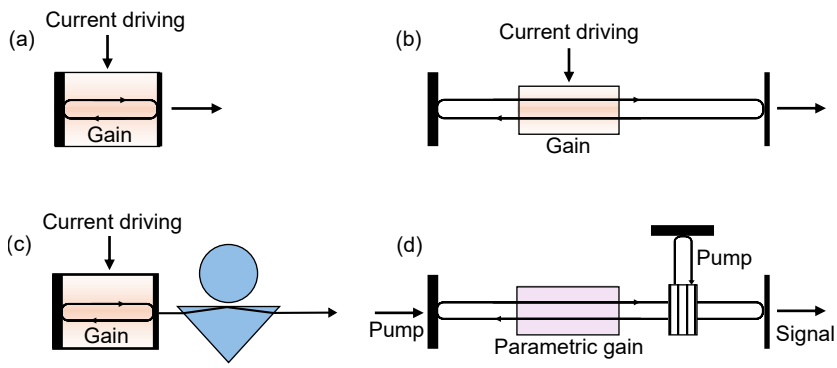

Figure 1.1: (a) Schematic of a conventional semiconductor laser. (b) Schematic of an external cavity semiconductor laser. (c) Schematic of a self-injection locked semiconductor laser. The blue structure represents a microsphere resonator with a coupling element. The microsphere resonator can provide a weak feedback to the semiconductor laser due to backscattering. (d) Schematic of an OPO with an external cavity. The structure with stripes represents a frequency selective element for separating the pump and signal waves.

Limited by the short cavity length and high absorption loss of active

materials, the linewidth of short-cavity semiconductor lasers based on intracavity feedback is still higher than MHz [22]. In order to reduce the laser linewidth, researchers introduced an external passive cavity structure [23, 24]. Based on the semiconductor gain chip, the cavity is extended outside the laser chip by using external mode selection elements or reflectors shown in Fig. 1.1(b). Compared with the intracavity feedback semiconductor laser, an external cavity can obtain narrower linewidth and wider wavelength tuning range by relying on its longer cavity length and more flexible tuning components in the external cavity. In 1993, researchers achieved a fine adjustment of the laser frequency by fine-tuning the external cavity length [25]. Through special designs of the external cavity, the intrinsic linewidth of semiconductor lasers can be suppressed to kHz or below [26, 27].

Around the same time, the self-injection locking (SIL) mechanism was also proposed [28, 29]. This method introduces a weak external optical feedback to interfere with the light in the laser cavity. The two signals will be phase coupled and the laser frequency will be locked to the feedback, which can effectively reduce the random drift and noise of the laser frequency and prevent the laser from changing its frequency during the excitation process. With the development of semiconductor laser technology, self-injection locking technology has been increasingly used in semiconductor lasers. Around the 1990s, researchers achieved self-injection locking in semiconductor lasers, as shown in Fig. 1.1(c). By introducing an optical feedback into the laser cavity, the output frequency of the laser can be well stabilized and the linewidth can be significantly reduced [30]. With the continuous development of this technology, semiconductor lasers can reach sub-hertz intrinsic linewidth level [15].

Narrow-linewidth optical parametric oscillators

Most conventional narrow-linewidth lasers have their gain provided by stimulated emission, so their operating frequency is limited by the gain medium. Optical parametric oscillators (OPOs) derive their gain from nonlinear polarization and their operating frequency is limited only by the absorption properties of the nonlinear medium used and the wave phase matching capabilities [31, 32]. In principle, OPOs can achieve narrow linewidth and tunable coherent oscillators over an extended wavelength range.

Various approaches to achieve narrow linewidth for OPOs have been investigated over the past few decades. The most common approach is

to use frequency-selective elements such as intracavity etalons or gratings [33–35], as shown in Fig. 1.1(d), which is similar to external cavity technologies. The approach can narrow the line shape of the signal wave by several orders of magnitude and is compatible with broadband wavelength tuning.

Integrated narrow-linewidth optical sources

With the maturity of micro-nano processing technologies, optical waveguide platforms such as silicon (Si) [36,37], silicon nitride (Si_3N_4) [38–41], III-V materials [42, 43], lithium niobate [44, 45] and so on, have been greatly developed and provided low-loss propagation. Among them, Si_3N_4 platform has relatively low waveguide loss, low thermo-optical coefficient, compatibility with complementary metal–oxide–semiconductor (CMOS) processes, no influence of two-photon absorption in the telecommunications window, and high Kerr nonlinearity. Despite these advantages of Si_3N_4 in passive photonic components, it has an indirect bandgap and presents many issues when considering active photonic components such as lasers.

So far, the common approach is hybrid integration or heterogeneous integration, combining active photonic components with passive devices in Si_3N_4, Si, etc. Hybrid integration is the process that connects multiple fully processed chips into a single package at the final packaging stage [46–48]. The advantage is that the devices can be tested and characterized before integration. Heterogeneous integration is a process of bonding unpatterned thin films to a Si or Si_3N_4 wafer in a coarse alignment manner and then processing the entire wafer [49–51]. This process technology achieves wafer-level manufacturing, and avoids coupling alignment problems between different structures, thereby improving integration density and cost-effectiveness.

In recent years, researchers have used the above hybrid integration to make a passive external cavity on Si_3N_4 chips and package them together with active chips, using the ultra-low loss of Si_3N_4 external cavity to help reduce the laser intrinsic linewidth to tens of Hertz [46, 47, 52]. The on-chip external cavity still uses the relevant technical principles of the previous external cavity, but on-chip integration makes the laser system more compact, stable, and also makes the narrow-linewidth lasers with external cavities more practical.

In addition, by using self-injection locking technology to provide a weak feedback for semiconductor lasers through a low-loss Si_3N_4 mi-

croresonator, the intrinsic linewidth of the laser can be suppressed to below 1 Hz [48, 53], which is comparable to low-noise fiber lasers. If heterogeneous integration technology and dispersion-engineered Si_3N_4 microresonators are used, narrow-linewidth OPOs can be directly realized on a single chip [54]. In this case, the integration of III-V lasers with Si_3N_4 microresonators can provide higher stability and additional functions, and the performance is better than a single III-V laser [14, 55–58].

1.2 This thesis

This thesis mainly focuses on the research of integrated narrow-linewidth optical sources. There are two types of optical sources: lasers that exploit stimulated emission from active materials and optical parametric oscillators that exploit nonlinearities.

First, in order to realize a chip-based narrow-linewidth semiconductor laser, a low-loss passive external cavity can be used to increase photon lifetime, or self-injection locking can be used to provide a weak optical feedback for semiconductor lasers to stabilize the generated frequencies. In either case, an integrated platform with ultra-low propagation loss is required. Therefore, based on the existing ultra-low loss silicon nitride platform, we tried to reduce the roughness of the waveguide sidewall by depositing a thin blanket layer after dry etching, to further decrease the waveguide loss [Paper A].

In addition, when the microring resonator is too close to the bus waveguide, the intrinsic loss of the microring will be high due to the extra parasitic loss. However, through the bound states in the continuum effect, high intrinsic Q factors or high ratio of intrinsic Q to extrinsic Q can be achieved at some specific wavelengths [59]. By periodically modulating the waveguide loss, mode competition is suppressed, thereby realizing a high-power on-chip optical parametric oscillator [Paper B].

Finally, as mentioned above, self-injection locking technology is often used to realize narrow linewidth semiconductor lasers, but whether it can be used for an OPO remains a question. One of the frequencies filtered out from a microcomb-based OPO is fed back to the silicon nitride microring via an optical fiber. By self-injection locking the frequency, its frequency noise is diluted by the low-loss long optical fiber, thereby suppressing the intrinsic linewidth of the frequency [Paper C].

Thesis outline

In this thesis, Chapter 2 introduces the fundamentals of frequency noise and linewidth, analyzes the noise limits of two types of optical coherent oscillators (semiconductor lasers, soliton microcombs), and shows the self-heterodyne method for measuring linewidth. Chapter 3 presents two external cavity designs for semiconductor lasers (long waveguide based and microring based) and their corresponding intrinsic linewidth calculations. It also demonstrates self-injection locking both theoretically and experimentally. Chapter 4 briefly introduces waveguide loss limitations, ultra-low loss silicon nitride process flow. Chapter 5 provides a summary and future outlook.

Chapter 2

Frequency noise in optical coherent oscillators

This thesis focuses on the development of optical coherent oscillators with narrow linewidth. In spite of its intuitive character, the definition of the laser linewidth is an aspect that still today sparks significant interest in the community and does not have a single unique metric for its characterization. In this chapter, we discuss the main concepts that permit analyzing the frequency noise of an optical coherent oscillator, including the self-heterodyne technique used to measure quantitatively the linewidth of our lasers. Therefore, this chapter provides the theoretical foundation for establishing a comparative and quantitative assessment of laser linewidth among different optical coherent oscillators.

2.1 Frequency noise

In reality, the amplitude, phase or frequency of an oscillator is not constant over time, but fluctuates in an irregular manner that cannot usually be represented by an analytical function of time. These unwanted fluctuations are often called noise or jitter. In order to describe these fluctuations, statistical measurements must be applied.

2.1.1 Basics of frequency noise

In the optical oscillator model, the instantaneous output electric field and instantaneous frequency of the optical oscillator are written as [60]

$$E(t) = (|E_0(t)| + |\Delta E_0(t)|) \cdot \exp[j2\pi\nu_0 t + j\Delta\phi(t)], \tag{2.1}$$

$$\nu(t) = \nu_0(t) + \Delta\nu(t) = \nu_0(t) + \frac{\mathrm{d}\Delta\phi(t)}{2\pi \mathrm{d}t}. \tag{2.2}$$

$|E_0(t)|$ represents the amplitude of the electric field. $|\Delta E_0(t)|$ represents the random amplitude fluctuation around $|E_0(t)|$. Similarly, $\Delta\phi(t)$ and $\Delta\nu(t)$ are the random phase and frequency fluctuation, respectively. ν_0 is the center optical frequency.

The power spectral density (PSD) is a time-domain statistical representation of a random process - the Fourier transform of the autocorrelation function which reveals the similarity of the noise state at adjacent moments. So the stability of physical quantities such as intensity, frequency, and phase is usually expressed in the frequency domain by their PSD. The PSD represents the distribution of the average power of a physical quantity over a certain period of time as the Fourier frequency changes. It represents the power carried per unit frequency, in units of power per Hertz [61].

$$R_\nu(\tau) = \lim_{T\to\infty} \int_{-T}^{T} \Delta\nu(t+\tau)\Delta\nu(t)dt. \tag{2.3}$$

$$\begin{aligned} S_\nu(f) &= \int_0^\infty R_\nu(\tau)\exp(-j2\pi f\tau)d\tau \\ &= 2\int_{-\infty}^{\infty} R_\nu(\tau)\exp(-j2\pi f\tau)d\tau. \end{aligned} \tag{2.4}$$

$$S_\nu(f) = f^2 S_\phi(f). \tag{2.5}$$

$R_\nu(\tau)$ is the autocorrelation function of the frequency fluctuation $\nu(\tau)$. In practice, we are only interested in the positive Fourier frequency f, so here, $S_\nu(f)$ is the single-sided PSD of the frequency fluctuation. The PSD of the phase fluctuation $S_\phi(f)$ has a similar definition [61].

If the PSD is integrated over the entire frequency range, the total average power can be obtained. In essence, it reflects that the energy of different frequency components that constitute the signal is generally different, that is, the contribution of signal components of different frequencies to the total energy of the signal is generally unequal. This is why in the frequency domain the concept of spectral density is used to describe stability rather than spectrum. The former has direct physical

meaning within a finite measurement time and can be directly measured, while the latter only exists in theoretical analysis of infinite time samples and will not converge once the samples are truncated within a finite time, making it difficult to obtain directly in actual measurements.

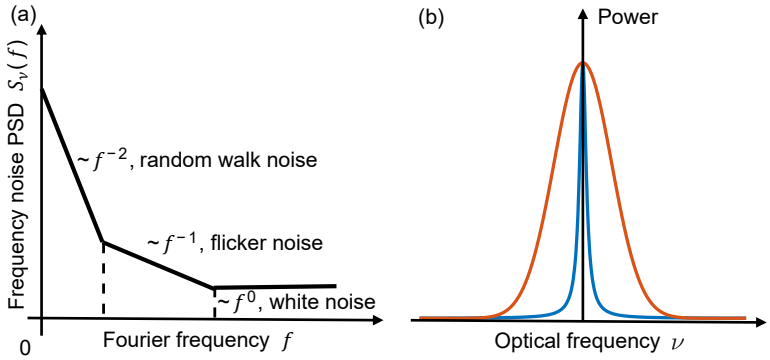

Figure 2.1: (a) Schematic of the frequency noise PSD of a single-frequency laser. Random walk noise and flicker noise dominate in the low frequency range (long-term stability), while white noise dominates in the high frequency range (short-term stability). Both axes are plotted on a logarithmic scale. (b) Schematic of the laser spectrum. At short time scales, the frequency spectrum is mostly a Lorentzian and very narrow (blue curve), while at longer time scales, when flicker noise kicks in, the centroid of the Lorentzian changes over time and the frequency spectrum looks broader, with a profile that resembles more a Voigt function (orange curve).

Typically, the frequency noise PSD $S_\nu(f)$ can be reasonably modeled by the superposition of three independent frequency noise processes that follow a power law with integer exponent $0 \leq \alpha \leq 2$ [60],

$$S_\nu(f) = \sum_{\alpha=0}^{2} h_\alpha f^{-\alpha}. \tag{2.6}$$

In the Fig. 2.1, the frequency noise PSD is divided into different regimes [62]. The contribution of low Fourier frequencies decreases with increasing frequency and includes random walk noise and flicker noise (also called 1/f noise). In the high frequency regime, PSD of the frequency fluctuations is usually independent of frequency and called white noise. For lasers, the random walk noise is caused by the influences of environment like temperature, vibrations. The flicker noise can be introduced by thermal noise within the laser cavity. The white noise

is caused by the random processes of spontaneous emission and carrier fluctuations [60].

2.1.2 Spectral line shape

Due to the frequency noise, the frequency spectrum distribution is no longer an ideal single line, but extends to both sides of the optical carrier frequency in the form of modulated sidebands, as shown in Fig. 2.1(b). The frequency noise PSD can provide a lot of information about laser noise, however, some experiments require a more complete understanding of the laser frequency fluctuations. Knowing the frequency noise PSD allows us to recover the laser line shape and thus the linewidth. Therefore, the relationship between the frequency noise PSD and the laser linewidth is discussed below.

By integrating over the full Fourier frequency range, the laser light field PSD or the laser line shape can be calculated directly from the laser frequency noise as follows [62–64]

$$S_E(\nu) = E_0^2 \int_0^\infty \cos[2\pi(\nu-\nu_0)\tau] \times \exp[-2\int_0^\infty S_\nu(f)\frac{\sin^2(\pi f\tau)}{f^2}df]d\tau, \tag{2.7}$$

where $S_E(\nu)$, $S_\nu(f)$ are the single-sided PSD of electric field and frequency noise, respectively.

In the absence of low frequency noise, $S_\nu(f) = h_0$ Hz^2/Hz and

$$S_E(\nu) = E_0^2 \frac{h_0}{(\nu-\nu_0)^2 + (\pi h_0/2)^2}. \tag{2.8}$$

It leads to the Lorentzian line shape with a full width at half-maximum (FWHM) of πh_0 Hz. The Lorentzian linewidth is also referred in the literature as fundamental linewidth or intrinsic linewidth [62].

If there is no high frequency noise, in the low frequency region (0, f_c], $S_\nu(f) = h_0$ Hz^2/Hz, and

$$S_E(\nu) = E_0^2(\frac{2}{\pi h_0 f_c})^{1/2}\exp[-\frac{(\nu-\nu_0)^2}{2h_0 f_c}]. \tag{2.9}$$

The line shape is Gaussian with a FWHM of $[8\ln(2)h_0 f_c]^{1/2}$ Hz that depends on the cutoff frequency f_c [63].

Combining the influence of the above frequency noises, the overall line shape has a Voigt-like profile like Fig. 2.2(b) [65]. The FWHM of the Voigt profile is called integrated linewidth [63]. The actual noise

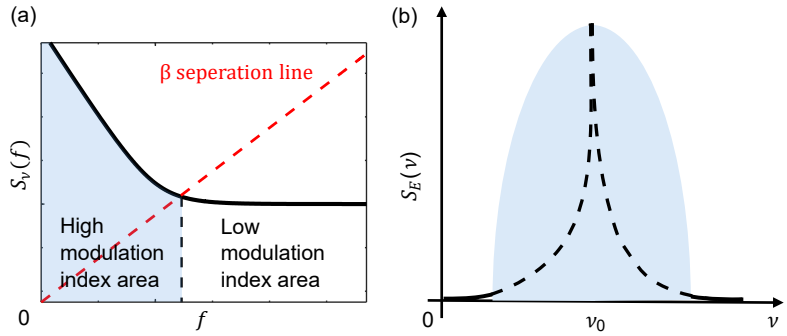

Figure 2.2: (a) Frequency noise PSD of a single-frequency laser. Both axes are plotted on a logarithmic scale. (b) Optical field PSD of the laser. The frequency line shape of the laser is approximately Gaussian in the center frequency (ν_0) part and Lorentzian on both sides.

spectrum of a laser is much more complex and produces line shapes that cannot be resolved and can only be determined by numerical methods. According to [63], the frequency noise PSD can also be divided into two regions using an approximate line (β separation line). As shown in Fig. 2.2, in the first region, $f < 8\ln(2) \cdot S_\nu(f)/\pi^2$ and the noise level is high compared to the Fourier frequency f. It contributes more to the integrated linewidth, this is to say, it provides a high modulation index. While $f > 8\ln(2) \cdot S_\nu(f)/\pi^2$, the noise contributes to the wings of the Lorentzian line shape or the intrinsic linewidth. The modulation speed of the frequency noise is too fast to have a significant effect on the integrated linewidth. The approximate value of the integrated linewidth follows the formula:

$$\mathrm{FWHM} = [8\ln(2)A_s]^{1/2}, \tag{2.10}$$

where A_s is the surface area of the high modelation index area (shaded area in Fig. 2.2(a)).

Figure 2.3 shows the frequency noise PSD of a semiconductor laser (CTL 1550) from TOPTICA measured using self-heterodyne method. It can be seen from the figure that the PSD value tends to be flat after 50 kHz. By calculating the average value of PSD from 50 kHz to 10 MHz as h_0, the intrinsic linewidth of this laser is around 190 Hz. Then calculate the shaded area and use Eq. 2.10 to get the integrated linewidth of 179 kHz. It can be said that the frequency noise PSD is convenient to assess the linewidth dynamics at different time scales.

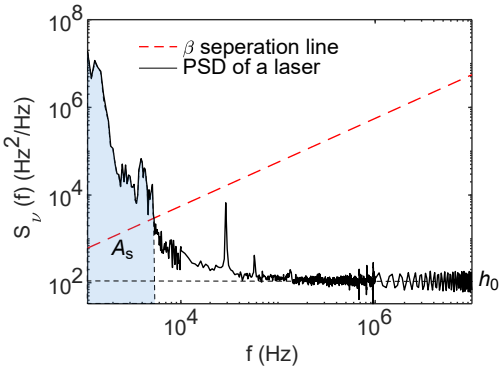

Figure 2.3: Measured frequency noise PSD of a semiconductor laser.

2.2 Linewidth theories of optical coherent oscillators

For high-speed applications such as data communications, the laser noise characteristics at high frequencies are more important because this noise regime mainly affects the phase error variance of the coherent communication link [66]. In this case, the intrinsic linewidth is more applicable. The target topic discussed in this thesis is the intrinsic linewidth. Therefore, the influencing factors and calculation of the intrinsic linewidth of semiconductor lasers and optical parametric oscillators will be introduced below.

2.2.1 Linewidth theory of semiconductor lasers

The linewidth of a single-frequency laser is determined by the quantum process of spontaneous emission. Each photon emitted spontaneously into the laser mode can induce stimulated emission and the resulting field amplitude is added to the field in the laser. Due to the statistical fluctuation contribution of the spontaneously emitted photons, the phase of the optical field in the laser cavity will fluctuate greatly, resulting in a large intrinsic linewidth [67].

Firstly, assuming that the laser is based on a FP cavity, the steady-state condition for the laser cavity is given by [68, 69]

$$r_1 r_2 \exp[2jkL + (g - \alpha_c)L] = 1, \tag{2.11}$$

where r_1, r_2 are the electric field reflectivities of the front and back facet, k is the propagation constant, L is the physical length of the cavity, g is

the modal gain and α_c is the loss due to absorption and scattering in the laser medium. From the real part of the above formula, the threshold modal gain g_{th} can be written by

$$\begin{aligned} g_{\text{th}} &= \alpha_c + \frac{1}{L}\ln(\frac{1}{r_1 r_2}) \\ &= \alpha_c + \alpha_m = \alpha_{\text{tot}}, \end{aligned} \tag{2.12}$$

where α_m is the facet loss of the two mirrors.

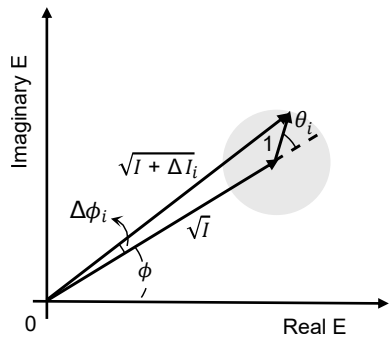

Figure 2.4: Vector-based description of the electric field under noise perturbation. I and ϕ represent the intensity and phase of the electric field, respectively. The initial electric field $E = \sqrt{I} \cdot \exp(j\phi)$, the random change $\Delta E = \exp(j\theta_i)$ caused by the i-th spontaneous radiation, and unit amplitude fluctuation is assumed. The instantaneous electric field $E = \sqrt{I + \Delta I_i} \cdot \exp(j\phi + j\Delta\phi_i)$.

Fig. 2.4 shows the electric field vector of each photon. The shaded area represents the random electric field fluctuation of the photon, including amplitude and phase fluctuations. The phase change $\Delta\phi_i$ of the photon is the result of the combined effect of the random phase change θ_i and the delayed phase change caused by the instantaneous change of the field intensity.

From a physical standpoint, the phase of the photon electric field is related to the real part of the medium's refractive index, while the imaginary part of the medium's refractive index affects the intensity of the photon electric field by affecting the net gain. Therefore, the phase change of the photon electric field in a laser is related to the changes in both the real and imaginary parts of the medium's refractive index, and the phase change caused by the change in light intensity or the imaginary part of the refractive index is additional.

In semiconductor lasers, the intensity change or the photon number change caused by spontaneous emission will cause a change in the carrier

density of the semiconductor active medium, and the carrier density change modifies the refractive index of the medium, thereby introducing the additional phase change. Compared with other types of lasers whose intensity fluctuation has little effect on the refractive index, the coupling between the amplitude and phase of the electric field is more pronounced in semiconductor lasers [68]. In this sense, this is the reason why the intrinsic noise or linewidth of semiconductor lasers is enhanced.

Here a linewidth enhancement factor α is introduced as [19, 70]

$$\alpha = \frac{\Delta n_{\text{real}}}{\Delta n_{\text{imag}}}. \tag{2.13}$$

Δn_{real}, Δn_{imag} are the fluctuations of the real and imaginary part of the refractive index $n = n_{\text{real}} - jn_{\text{imag}}$. α is related to the active medium. And then, combined with the rate equations [19], the phase change $\Delta\phi_i$ can be expressed as

$$\Delta\phi_i = -\frac{\alpha}{2I} + \frac{1}{\sqrt{I}}(\sin\theta_i - \alpha\cos\theta_i), \tag{2.14}$$

where $\theta_i \in (0, 2\pi]$, $I = |E|^2$ is the field intensity. The first term is a small but constant phase shift that can be ignored. Therefore, the total phase fluctuation for spontaneous emission is

$$\Delta\phi = \sum_{i=1}^{N} \frac{1}{\sqrt{I}}(\sin\theta_i - \alpha\cos\theta_i), \tag{2.15}$$

where N is the number of spontaneous emission in a certain duration. After a series of deductions, the intrinsic linewidth of semiconductor laser becomes [19, 71, 72]

$$\Delta\nu = \frac{v_g^2 h\nu_0 n_{\text{sp}}\alpha_m\alpha_{\text{tot}}(1+\alpha^2)}{4\pi P_{\text{tot}}}, \tag{2.16}$$

where v_g is the group velocity of the laser, and h is the Planck constant ($6.62607015 \times 10^{-34}\text{J}\cdot\text{s}$). n_{sp} is the spontaneous emission factor, whose physical meaning is the proportion of spontaneous emission entering the laser modes [61]. α_c and α_{tot} are the propagation loss and total loss of the laser cavity, respectively, as shown in Eq. 2.12. P_0 is the output power per facet, and the total output power $P_{\text{tot}} = 2P_0$, if $r_1 = r_2$.

It can be seen that the intrinsic linewidth is inversely proportional to the output power. Fig. 2.5 shows the measured intrinsic linewidth of

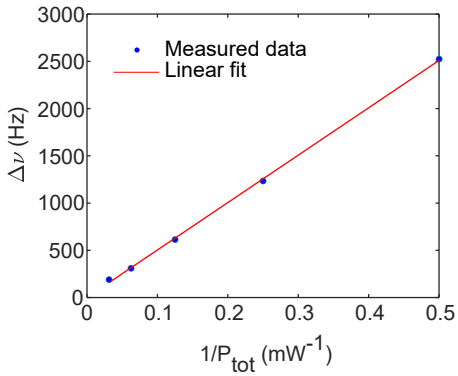

Figure 2.5: The relationship between the intrinsic linewidth $\Delta\nu$ of a semiconductor laser and the output power P_{tot}.

a semiconductor laser at different output powers (2, 4, 8, 16, 32 mW). The intrinsic linewidths are obtained by measuring the PSD of white frequency noise using the method in the previous section. The other parameters such as wavelength and temperature are fixed, and the output power is changed only by changing the driving current. The measured data is basically consistent with the fitted data.

In addition, in order to obtain a narrow linewidth for a given output power, α_m and α_c should be as low as possible [73]. According to Eq. 2.12, if the reflectivities of two facets r_1, r_2 are unchanged, extending the cavity length L can effectively reduce α_m. α_c is the propagation loss of the cavity, which depends strongly on the material, design and manufacturing method. Decreasing the propagation loss can also reduce the laser intrinsic linewidth.

2.2.2 Linewidth theory of optical parametric oscillators based on soliton microcombs

Since the lasing wavelength of a laser depends on the bandgap of the active material, currently relying solely on lasers as light sources may not be able to cover the entire optical band, which limits optical applications and researches. An OPO is based on optical parametric amplification, and its gain wavelength is no longer limited by the material bandgap, so the optical bands that cannot be covered by lasers can be achieved by OPOs. As a special and practical OPO, a microcomb has been increasingly studied. Microcomb is an optical frequency comb generated in a nonlinear high-Q microcavity, which is widely used in

high-precision time and frequency measurement, optical communication and other fields [74–76]. It uses four-wave mixing (FWM) to generate multiple equally spaced frequencies [77].

Conventional frequency combs are based on mode-locked lasers [78], where the gain of a conventional frequency comb comes from stimulated emission in the active gain medium, so its intrinsic linewidth is partially determined by spontaneous emission. In contrast, the gain of soliton microcombs is based on optical parametric amplification, and the noise caused by spontaneous scattering is very weak. The pump laser is added to the microcombs in a coherent manner, so its noise is uniformly transmitted to all comb lines [79].

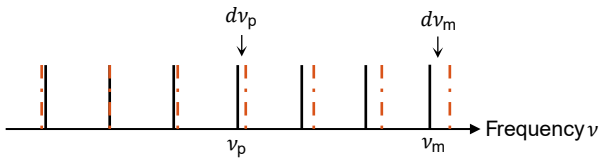

Figure 2.6: Schematic of the comb line distribution and the repetition rate change caused by the change of pump frequency. ν_p, ν_m are the frequencies of pump and m-th comb line. The black line segments represent the initial comb lines, and the red dashed line segments represent the comb lines after the pump frequency is shifted.

Fig. 2.6 shows the distribution of the comb lines. The frequency of the m-th comb line can be expressed as

$$\nu_m = \nu_p + m\nu_{\text{rep}}, \tag{2.17}$$

where m is counted from the pump, and ν_p, ν_{rep} are the pump frequency and the repetition rate of the frequency comb. If the repetition rate remains exactly the same, the pump frequency noise will be transferred to each comb line. However, the pump frequency noise can also affect the repetition rate due to intrinsic intra-pulse Raman scattering [80] and dispersive wave recoil [81]. Therefore, a linear perturbation on Eq. 2.17 results into

$$d\nu_m = d\nu_p(1 + m\frac{d\nu_{\text{rep}}}{d\nu_p}), \tag{2.18}$$

where $d\nu_p$ is the pump frequency fluctuation, $d\nu_m$ and $d\nu_{\text{rep}}$ are the changes in m-th comb line frequency and repetition rate caused by pump frequency fluctuation. According to experimental studies [82], $d\nu_{\text{rep}}$ is positively proportional to $d\nu_p$. If the pump light has a positive frequency

offset, the repetition rate will increase. As shown in Fig. 2.6, for comb lines with higher frequencies than the pump, the frequency offset increases with increasing frequency. On the other side of the pump, there may be some comb lines with a smaller frequency offset than the pump.

Because the PSD (calculated by Eq. 2.4) can be used to calculate the linewidth of an optical source, the frequency noise PSD of the m-th comb line $S_{\nu,m(f)}$ is calculated as [82]

$$S_{\nu,m}(f) = S_{\nu,p}(f)(1 + m\frac{d\nu_{\text{rep}}}{d\nu_p})^2. \tag{2.19}$$

$S_{\nu,p}(f)$ is the PSD of the pump frequency noise. It can be seen that the intrinsic linewidth of the microcomb due to pump frequency noise has a parabolic relationship with the number of comb lines.

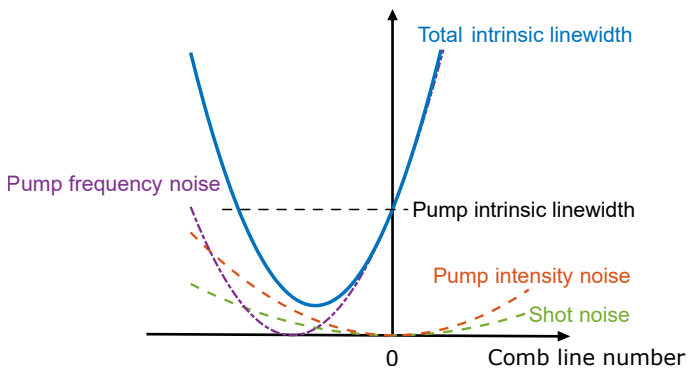

Figure 2.7: Schematic of intrinsic linewidth contribution of a soliton microcomb. Comb line 0 represents the pump frequency.

In addition to the pump frequency noise, the pump intensity noise and shot noise also affect the intrinsic linewidth of the comb lines. As shown in Fig. 2.7, the three noise sources are independent of each other and all introduce a parabolic distribution to the intrinsic linewidth [82–84]. The difference is that the linewidth distribution caused by the pump intensity noise and the shot noise is symmetric about the pump frequency, and the two contributions are usually weaker than the pump frequency noise. After adding them together to get the total intrinsic linewidth, there will still be some comb lines with an intrinsic linewidth narrower than the intrinsic linewidth of the pump frequency.

Fig. 2.8 shows the optical spectrum and corresponding intrinsic linewidth distribution of a soliton microcomb generated on a Si_3N_4 microring resonator with a free spectral range (FSR) of 100 GHz. Since a

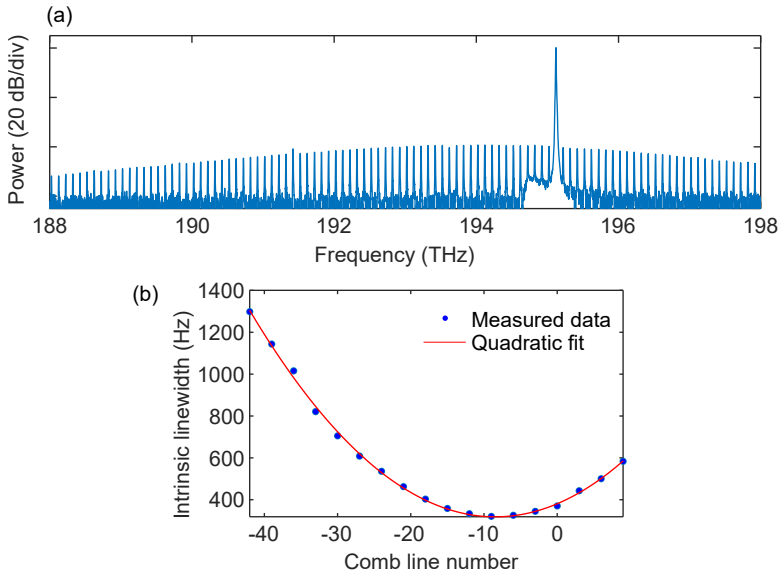

Figure 2.8: (a) Frequency spectrum of a soliton microcomb. (b) Measured and fitted intrinsic linewidth distribution.

sufficient power is required for linewidth measurement, an erbium-doped fiber amplifier (EDFA) is used to amplify the power of the comb lines. The total number of comb lines which can be measured is limited by the bandwidth of the EDFA. Nevertheless, comb lines from -42 to 9 can be measured. One can see that the intrinsic linewidth has an almost perfect parabolic profile, and the intrinsic linewidths of comb lines -16 to -1 are below that of the pump frequency.

In the experimental data of [Paper C], a parabolic distribution of the intrinsic linewidth of the soliton microcomb can be also observed regardless of whether there is optical feedback or not. Because the shape of the parabola can be directly determined by two points, and the linewidth of the pump is constant, only one frequency can be fed back to the main cavity. However, if the optical frequency line can be far away from the pump frequency, a low-linewidth multi-wavelength light source with a broad bandwidth can be realized.

2.3 Self-heterodyne method

The self-heterodyne method is one of the most widely used laser linewidth measurement techniques, especially for characterizing the co-

herence of optical oscillators [85]. This method relies on the interference principle to determine the frequency information by comparing the laser signal with its delayed signal. The following is a brief introduction to the principle, experimental steps, advantages and disadvantages of this method.

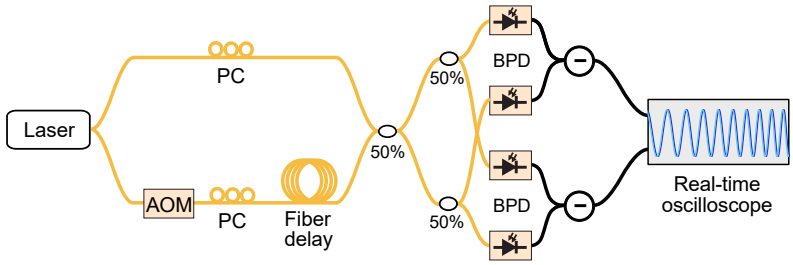

Figure 2.9: Schematic of the correlated self-heterodyne measurement setup. PC: polarization controller, AOM: acousto-optic modulator, BPD: balanced photodetector.

As shown in Fig. 2.9, the laser signal is first split using a beam splitter. One of the split signals is sent directly to the measurement system as a reference. The other path is delayed in time and optionally shifted in frequency by an acousto-optic modulator (AOM). The AOM is driven with a 80 MHz radio-frequency carrier, and the sampling rate of the oscilloscope is set to 625 MHz to prevent aliasing. A time delay is introduced in the delayed path, which can be controlled by changing the optical fiber length. The two outputs are split and received by two identical balanced photodetectors (BPDs). Using BPDs helps suppress relative intensity noise (RIN) and allows for cross-correlation between the electrical outputs, thereby suppressing the independent BPD noise [86]. The two signals interfere with each other and generate a beat signal whose spectral properties depend on the laser linewidth. A wider laser linewidth corresponds to a more significant frequency fluctuation between the two signals. By analyzing the PSD of this beat signal, the linewidth information can be extracted [86–88].

When performing the experiment, careful attention must be paid to the system design. When the fiber delay is long enough, the two interference paths will experience different phase changes, causing their interference effect to be clearly visible. In this way, by comparing the interference signals, the spectral information of the laser can be obtained. We used the delayed fiber with the length of 1.5 km.

It is relatively simple and easy to implement, as this method only requires standard optical components such as beam splitters and delay paths. More important thing is that it does not require an external reference frequency, providing flexibility in experimental design. At the same time, it has high sensitivity and can accurately detect frequency fluctuations, making it suitable for measuring narrow linewidths [85]. According to the measured results in [Paper C], the measurement system can measure an intrinsic linewidth down to approximately 0.1 Hz.

However, it also has some disadvantages. One limitation is the need for sufficiently long time delays and the accuracy of the method depends on the stability of the laser signal or other measurement components. This measurement system is sensitive to environmental interference or other system fluctuations. Since our measurement system is not vibration proof or temperature-controlled, and considering the storage space of the oscilloscope, we believe that the frequency noise above 1 kHz in the Fourier frequency is credible, as shown in Fig. 2.3. Finally, data analysis requires advanced signal processing methods [86].

In summary, the self-heterodyne method is a mature and practical linewidth measurement method with high sensitivity and wide applicability, but it requires appropriate experimental setup and attention to the data processing methods. With careful design and implementation, this method can provide accurate and reliable laser linewidth measurements.

Chapter 3

Narrow-linewidth lasers and self-injection locking

In the previous chapter, we mentioned that the intrinsic linewidth is more applicable and this thesis mainly discusses the intrinsic linewidth. In practical experiments, electrical feedback and locking techniques are often used to reduce the linewidth of light sources They are very effective for reducing low-frequency linewidth, but due to bandwidth limitations, these techniques are less effective for high frequency noise [62]. Therefore, it is necessary to use optical strategies to suppress the intrinsic noise of light sources. This chapter introduces two common optical methods: external cavity lasers and self-injection locking.

3.1 Narrow-linewidth lasers with external cavities

According to the description in Section 2.2.1, the intrinsic linewidth of a semiconductor laser is related to the intracavity propagation loss and cavity length. As can be seen from Eq. 2.16, when other parameters are constant, a longer cavity length has a suppressive effect on the intrinsic noise of a semiconductor laser. However, the propagation loss of active media is relatively high. Simply increasing the length of the active media cannot significantly reduce the intrinsic linewidth. Therefore, semiconductor lasers are often combined with low-loss passive external cavities to achieve narrow linewidth.

The configuration of a semiconductor laser with an external cavity is shown in Fig. 3.1. The external mirror can be expressed by $r_3(\omega)$

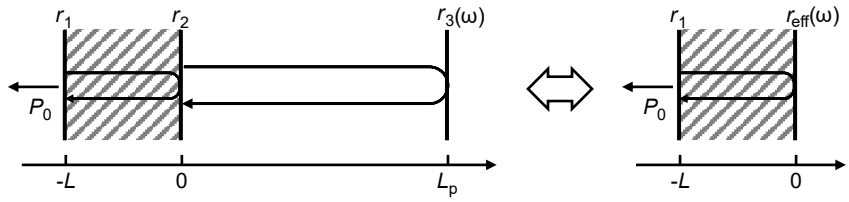

Figure 3.1: Schematic of a semiconductor laser with an external cavity and its equivalent structure. The output power P_0 is emitted from the front mirror. The electric field reflectivities of the laser mirrors and external mirror are r_1, r_2, $r_3(\omega)$. r_1, r_2 may have weaker wavelength dependence, but we ignore it here. The physical length of the laser cavity is L and the passive external cavity is L_p.

which could be a frequency-dependent electric field reflectivity [89], such as Bragg grating [51], multiple microrings [49], and so on. Generally, the propagation loss of the external cavity is much lower than that of the laser waveguide. Compared to simple FP lasers, the complexity of the external cavity is relatively high. In order to use the theoretical predictions in Section 2.2.1, the passive external cavity can be replaced by an effective mirror with a complex wavelength dependence, denoted as [62]

$$\begin{aligned} r_{\text{eff}}(\omega) &= t_2^2 \cdot t_{\text{passive}}(\omega)^2 \cdot r_3(\omega) \\ &= (1 - r_2^2) \cdot \exp(-j\omega\tau_p - \alpha_p L_p) \cdot r_3(\omega), \end{aligned} \tag{3.1}$$

where τ_p is the round-trip time of the external cavity. The propagation loss of the passive external cavity is α_p. The effective reflectivity r_{eff} is the transfer function of the round-trip transmission of the entire passive cavity. This term can be separated into amplitude and phase as

$$r_{\text{eff}}(\omega) = |r_{\text{eff}}(\omega)| \exp[j\varphi_{\text{eff}}(\omega)]. \tag{3.2}$$

And the total losses of the semiconductor laser is

$$\begin{aligned} \alpha_{\text{tot}} &= \alpha_c + \alpha_m \\ &= \alpha_c + \frac{1}{L}\ln(\frac{1}{r_1 \left|r_{\text{eff}}(\omega)\right|}). \end{aligned} \tag{3.3}$$

According to Eq. 2.16 in Chapter 2, combined with the above effective reflectivity, the intrinsic linewidth becomes [16, 62, 89]

$$\Delta\nu = \frac{v_g^2 h\nu_0 n_{\text{sp}} \alpha_m \alpha_{\text{tot}} (1+\alpha^2)}{4\pi P_0 \left[1 + \frac{r_1}{|r_{\text{eff}}(\omega)|} \frac{1-|r_{\text{eff}}(\omega)|^2}{1-r_1^2}\right]} \cdot \frac{1}{F^2}, \tag{3.4}$$

where P_0 is the output power emitted by the front mirror with reflectivity r_1. Due to the frequency dependence of the phase and reflectivity of the external cavity, the intrinsic linewidth is reduced by F^2 [52, 90].

$$F = 1 + A + B, \tag{3.5}$$

where

$$A = \frac{1}{\tau_0} \frac{d\varphi_{\text{eff}}(\omega)}{d\omega}, \tag{3.6}$$

$$B = \frac{\alpha}{\tau_0} \frac{d(\ln |r_{\text{eff}}(\omega)|)}{d\omega}. \tag{3.7}$$

$\tau_0 = 2L/v_{\text{g}}$ is the round-trip time in the semiconductor laser cavity. A can be thought of as the ratio of the round-trip times between the passive external cavity and the laser cavity. From this perspective, the longer the passive cavity, the stronger the linewidth suppression. Due to the existence of the factor α, B will only appear when α is non-zero. B represents the additional linewidth suppression mechanism based on the coupling of light field intensity and phase in semiconductor lasers [52].

3.1.1 Long-waveguide based external cavity

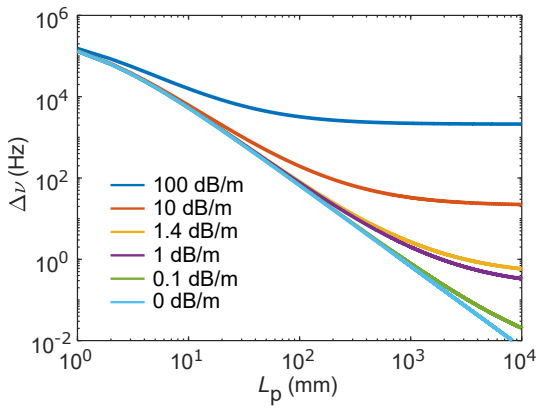

Figure 3.2: Intrinsic linewidth calculation based on different external cavity losses α_p and lengths L_p. Parameters used in the simulation: $\alpha = 5$, $n_{\text{sp}} = 2$, laser wavelength $\lambda = 1550$ nm, output power $P_0 = 1$ mW, length of active part $L = 0.7$ mm, group index $n_{\text{g,active}} = 3.6$, $n_{\text{g,passive}} = 2$, reflection coefficients $r_1 = 0.9$, $r_2 = 0.9$, $r_3 = 1$, propagation loss of active part $\alpha_c = 13$ cm^{-1}.

Consider a semiconductor laser with a long external waveguide and a frequency-independent external mirror ($dr_3(\omega)/d\omega = 0$, $d|r_{\text{eff}}(\omega)|/d\omega =$

0, $B = 0$). Based on Eq. 3.4, the intrinsic linewidth of that laser can be calculated. As shown in Fig. 3.2, for the same waveguide loss, the intrinsic linewidth decreases as the external cavity becomes longer, which is consistent with the above discussion.

However, the suppression is finally limited by the propagation loss in the external cavity. If the passive external cavity has no propagation loss, the intrinsic linewidth of the laser will decrease endlessly. But when the passive external cavity has a certain propagation loss, the intrinsic linewidth of the laser will gradually converge as the physical length of the external cavity increases. Light continues to lose energy in a lossy extended cavity until its energy is substantially lost, at which point there is no longer any benefit from increasing the external cavity length. Due to the different propagation loss in the external cavity, the cavity length is also different when the intrinsic linewidth converges.

In general, increasing the length of the passive external cavity is very effective in reducing the intrinsic linewidth of the semiconductor laser, but the propagation loss of the cavity ultimately determines the effectiveness of this method.

3.1.2 Microring based external cavity

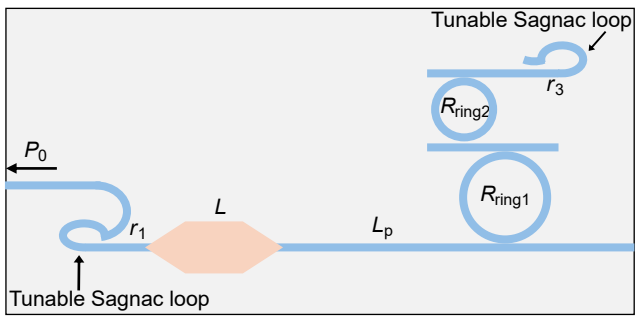

Figure 3.3: Schematic of an on-chip external cavity semiconductor laser based on multi-rings. The polygon with length L represents the active part, and the blue structures represent the passive part. The two mirrors are tunable Sagnac loops, and the reflection coefficients r_1, r_3 can be adjusted by thermal methods using metal microheaters. The waveguide connecting the active part and ring1 can also be heated to change the phase shift, and its length is L_p. The lengths of the two Sagnac rings are negligible. The radii of the two microrings are R_{ring1} and R_{ring2}, respectively, where R_{ring1} is slightly larger than R_{ring2}.

If the external mirror is a Bragg grating or multi-rings, as shown in

Fig. 3.3, the reflectivity will be frequency-dependent. Here, in the above case, $|r_{\text{eff}}|$ is frequency-independent, so $B = 0$. By adding the frequency selective mirror, B is increased at certain wavelengths, so the intrinsic linewidth is further suppressed.

The calculation of r_{eff} depends on the designs of the external cavities. In the case shown in Fig. 3.3, r_{eff} is expressed as

$$r_{\text{eff}}(\omega) = t_2^2 \cdot t_{\text{passive}}(\omega)^2 \cdot t_{\text{ring1}}(\omega)^2 \cdot t_{\text{ring2}}^2(\omega) \cdot r_3, \tag{3.8}$$

where t_2 is the coupling between the active waveguide with the passive waveguide. t_{passive}, t_{ring1}, t_{ring2} are the electric field transmission coefficients of the passive phase shifter with the length of L_p, the two microrings.

At the same time, the effective cavity length L_{eff} can also be obtained by calculating the time delay of the entire external cavity. Because the time delay is calculated based on the round-trip time, half the round-trip time should be used when calculating the effective cavity length.

$$L_{\text{eff}}(\omega) = \frac{d\varphi_{\text{eff}}(\omega)}{d\omega} \cdot \frac{v_{\text{g,passive}}}{2}. \tag{3.9}$$

Based on the above equations, the external effective reflectivity r_{eff}, effective cavity length L_{eff}, coefficients A, B, F and intrinsic linewidth $\Delta\nu$ are calculated as shown in Fig. 3.4. Because the effective reflectivity r_{eff} of the external cavity is wavelength selective, the external reflector has strong reflection only at the resonant wavelength shared by the two microrings, which means that the loss of the external cavity is low at the wavelength. The two microrings have slightly different sizes, so the FSR caused by the Vernier effect is quite large. This undoubtedly filters the original broadband active gain again in the wavelength selection of the entire cavity. Similar to r_{eff}, the effective length L_{eff} is also symmetric with the common resonant wavelength and is maximum at the wavelength, which is much longer than the physical length of the external cavity.

In addition, since the effective length of the external cavity is maximum at the common resonant wavelength, the factor A is maximum at the same location. The factor B is proportional to $d\ln|r_{\text{eff}}(\omega)|/d\omega = d(\alpha_p L_{\text{eff}})/d\omega$, which corresponds to the derivative of the effective length L_{eff} with respect to frequency [49, 52, 91], so it is centrally symmetric and its maximum is located at longer wavelength than the common resonance. Under the combined effect of A and B, the maximum F is also

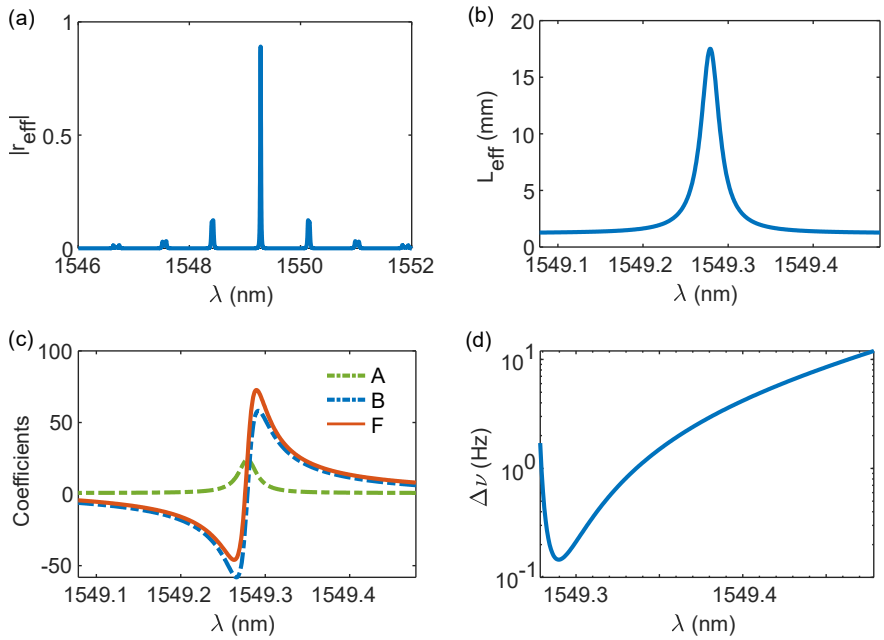

Figure 3.4: (a) Magnitude of the effective reflectivity r_{eff}. (b) Effective length L_{eff} of the external cavity. (c) Coefficients A, B, F. (d) Theoretically estimated intrinsic linewidth $\Delta\nu$. They are all related to the laser wavelength λ. Parameters used in the simulation: $\alpha = 5$, $n_{\text{sp}} = 2$, output power $P_0 = 1$ mW, lengths of active, passive parts $L = 0.7$ mm, $L_p = 1$ mm, group index $n_{\text{g,active}} = 3.6$, $n_{\text{g,passive}} = 2$, reflection coefficients $r_1 = 0.9$, $r_3 = 1$, propagation losses of active, passive parts $\alpha_c = 13$ cm^{-1}, $\alpha_p = 2$ dB/m, the coupling coefficient between microrings with bus waveguides $\kappa = 0.09$, radii of two microrings $R_{\text{ring1}} = 250$ μm, $R_{\text{ring2}} = 240$ μm. Coupling loss between the active part with the passive part is 0.5 dB, so $t_2 = 10^{(-0.5/20)}$.

located on the long wavelength side of the resonant wavelength, and the optimal intrinsic linewidth can be obtained at the maximum F point. In other words, the linewidth suppression induced by effective mirror feedback can theoretically perform better when the laser wavelength is slightly increased relative to the common resonant wavelength.

Compared with long-waveguide based external cavities, the microring based external cavity is more complicated when calculating the effective reflectivity r_{eff}. On the one hand, the microring provides further wavelength selection for the external cavity, but its L_{eff} is similar to the waveguide length L_p in the long-waveguide based external cavity. The lower the propagation loss or the longer the L_{eff}, the better the sup-

pression effect on the intrinsic linewidth. It's just that the L_{eff} of the microring based external cavity is wavelength selective. At non-resonant wavelengths, the microrings are wasted because they are not utilized. At the resonant wavelength, the equivalent length brought by the microrings is longer than the physical length, and the suppression of the intrinsic linewidth is stronger. On the other hand, due to the wavelength selectivity of the microring, the factor B is non-zero, so it can provide additional suppression effect at certain wavelengths. Because of its wavelength selectivity, the operating frequency and phase shifter need to be finely adjusted during design or experiment.

3.2 Self-injection locking

For the semiconductor laser with the external cavity, the passive and active parts can be considered as a whole. The reflectors at both ends can be designed on the passive platform, and the active part is mainly responsible for providing optical gain. The lasing frequency is determined by the two parts. Without the passive part, the laser would have an extremely low Q factor, or even not be a laser due to the lack of reflectors built into the passive part. When a semiconductor laser is self-injection locked, the external feedback is mainly provided by the backscattering which is very weak [92–95]. The generated frequency is mainly determined by the semiconductor laser itself. Even without the external feedback, the laser still operates normally, just with higher phase noise. When the semiconductor laser is locked to the external resonator, the generated frequency is determined by the resonator. It can only be fine-tuned within a narrow wavelength range, otherwise the self-injection locking will be interrupted due to the large frequency difference of the two components. The following section will analyze the dynamics of self-injection locking.

3.2.1 Dynamics of self-injection locked lasers

The self-injection locking system is shown in Fig. 3.5. The laser operates at a single frequency and the instantaneous electric field $E(t) = |E(t)|\exp(j\phi)$ is reflected from the output mirror with the reflection coefficient of r_2. $E(t)$ is the sum of the electric field reflected from both mirrors and the electric field transmitted back to the laser cavity due to the backscattering in the microring resonator [96]. The backscattering

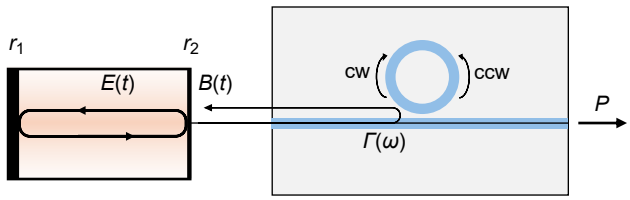

Figure 3.5: Schematic of a self-injection locked semiconductor laser. The reflectivities of the mirrors on both sides of the laser are r_1, r_2, and the electric field is $E(t)$. The laser is incident from the left side of the microring resonator and output from the right side. The electric field reflected by the microring is $B(t)$, and the reflection coefficient is $\Gamma(\omega)$. There are two modes in the microring resonator, one propagating in clockwise (cw) and the other propagating in counterclockwise (ccw), and they are coupled to each other.

is introduced by the inhomogeneity of the waveguide interface [97]. So the electric field in the laser cavity can be expressed as

$$\begin{aligned}|E(t)|\exp[j\phi(t)] = {} & jt_2B(t) \\ & + r_1r_2\,|E(t-\tau_0)|\exp[j\omega\tau_0 + j\phi(t-\tau_0) + (g-\alpha_c)L],\end{aligned} \tag{3.10}$$

where $t_2 = \sqrt{1-r_2^2}$ is the transmission coefficient, τ_0 is the round-trip time of the FP laser cavity, g is the gain coefficient, α_c is the propagation loss of the active medium, L is the laser cavity length, ω is the instantaneous angular frequency of the generated light, ω_d is the resonant angular frequency of the FP laser cavity. In the self-injection locking state, the frequency finally generated by the system may not be equal to the resonant frequency of the FP laser cavity, so ω is used instead of ω_d. Similarly, the reflected electric field $B(t)$ is

$$B(t) = \frac{jt_2\Gamma(\omega)}{r_2}|E(t-\tau_s)|\exp[j\omega\tau_s + j\phi(t-\tau_s)], \tag{3.11}$$

where τ_s is the round-trip time from laser coupling to the microring resonator, and $\Gamma(\omega)$ is the frequency-dependent reflection coefficient of the microring resonator. If the resonant angular frequency of the microring resonator is ω_m, combined with the steady-state expression [96],

$$\Gamma(\omega) = -\frac{j\eta\kappa_m^2\gamma/2}{(\kappa_m/2 - j(\omega-\omega_m))^2 + (\kappa_m\gamma/2)^2}, \tag{3.12}$$

where $\kappa_m = \kappa_{mi} + \kappa_{mc}$ is the total decay rate of the microring resonator, κ_{mi}, κ_{mc} are the intrinsic, extrinsic decay rate. $\eta = \kappa_{mc}/\kappa_m$, and γ is

mode-splitting coefficient related to the mutual coupling between the cw and ccw modes.

By taking the time-independent solutions (steady-state) for $E(t)$, $\phi(t)$ [95], and introducing the detuning of the laser cavity frequency from the microring resonant frequency $\xi = 2(\omega_d - \omega_m)/\kappa_m$, as well as the generation detuning of the generated frequency from the microring resonant frequency $\zeta = 2(\omega - \omega_m)/\kappa_m$, their relationship is as follows

$$\xi = \zeta + \frac{K}{2}\frac{2\zeta\cos\psi + (1+\gamma^2-\zeta^2)\sin\psi}{(1+\gamma^2-\zeta^2)^2+4\zeta^2}, \tag{3.13}$$

where $\psi = \omega\tau_s - \arctan\alpha + 3/2\pi$ is the phase delay (α is also linewidth enhancement factor). K is the combined coupling coefficient [96]. This relationship is usually called tuning curve as shown in Fig. 3.6.

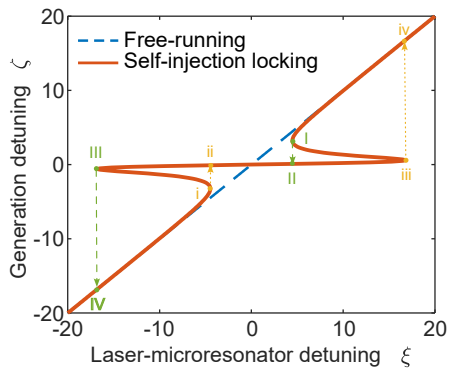

Figure 3.6: Tuning curve of a semiconductor laser locked to a microring resonator. The horizontal axis represents the difference between the laser resonant frequency and the microring resonant frequency, and the vertical axis represents the difference between the system output frequency and the microring resonant frequency.

For a free-running laser, the tuning curve is a straight line with a slope of 1 as shown by the blue dashed line, so the output wavelength is consistent with the laser resonant wavelength. For the self-injection locked laser, the tuning curve has an almost horizontal part (point III to iii). Tuning the laser cavity frequency ω_d from low to high so that it gradually approaches the microring resonant frequency ω_m, the generated frequency ω initially follows a straight line until the inflection point i. At the inflection point i, it jumps to the ultra-low slope part (point ii), achieving locking. In this range , the effect of adjusting the laser cavity frequency on the generated frequency can be ignored until the inflection

point iii arrives. In other words, within the locked region, the generated frequency will depend on the resonant frequency of the microring rather than the laser cavity frequency, which is called frequency pulling. The same is true when the frequency sweep direction is opposite. The width of the flat slope region is called the locking band.

In addition, the intrinsic linewidth reduction can also be seen from the tuning curve. After simplifying and differentiating Eq. 3.13, the linewidths of the free-running laser and the self-injection locked laser can be approximately expressed as [96]

$$\frac{\Delta\nu_{\text{locked}}}{\Delta\nu_{\text{free}}} = \frac{d\omega}{d\omega_d} = \frac{d\zeta}{d\xi} = \frac{Q_d^2}{Q_m^2}\frac{1}{16\Gamma_m^2(1+\alpha^2)}, \tag{3.14}$$

where Q_d, Q_m are the total Q factors (ratio of resonant frequency to decay rate) of the FP laser cavity and the microring resonator. Generally, the Q factor of a laser is lower than that of a microring resonator. The slope $d\zeta/d\xi$ of the flat region is a very small value. That is, the frequency fluctuation of the self-injection locked laser is many times smaller than that of the free-running laser. Therefore, self-injection locking can suppress the intrinsic linewidth of the laser [98, 99].

[Paper C] demonstrated a similar self-injection locking method, but the optical source is a soliton microcomb instead of a semiconductor laser, and the external resonator is a fiber loop. The Q factor of the fiber loop is much higher than that of the Si_3N_4 microring. After filtering out a frequency, inputting it into the fiber loop and feeding it back into the Si_3N_4 microring, the intrinsic linewidth of that frequency is also greatly suppressed.

3.2.2 Experimental study on self-injection locked lasers

Based on the integrated Si_3N_4 platform, self-injection locking is usually achieved by locking a semiconductor laser to a high-Q Si_3N_4 microring to suppress the linewidth of the laser [48, 56, 100, 101].

The experimental setup of a self-injection locked semiconductor laser is shown in Fig. 3.7(a). The half-packaged DFB laser has two pins for drive current and four pins for temperature control. The highest output optical power is around 80 mW at the driving current of 300 mA. The operating wavelength is usually 1550 nm, and the tunable wavelength range is about 0.5 nm. The operating wavelength can be tuned by changing the driving current or temperature of the laser. The former allows for more precise wavelength adjustment.

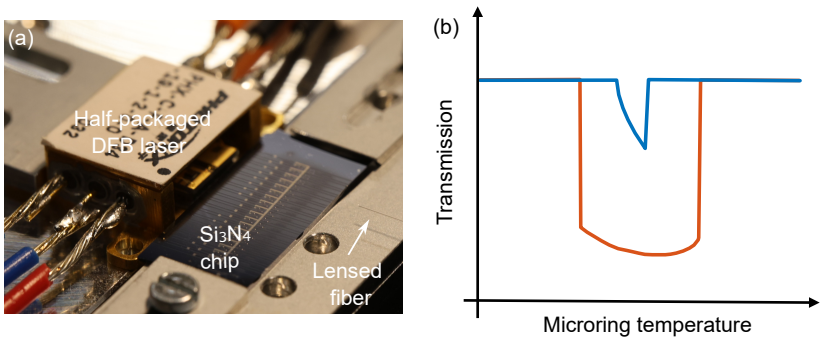

Figure 3.7: (a) Photos of experimental setup for self-injection locking. The DFB laser on the left is butt-coupled to the Si_3N_4 chip in the middle, and the light is then collected by the lensed fiber on the right. (b) Schematic of the transmission of the Si_3N_4 microring as the microring temperature. The microring temperature is controlled by a metal heater. The orange curve indicates an inappropriate phase shift between the DFB laser and the microring, and the blue curve indicates an appropriate phase shift.

The laser chip extends 1 mm out of the package to facilitate coupling with the Si_3N_4 chip. The laser's mode spot diameter is roughly 2.8 μm, slightly larger than the 2.5 μm mode spot diameter of the commonly used lensed fiber. However, the laser has a large vertical divergence angle. In order to improve the coupling efficiency, the distance between the Si_3N_4 chip and the DFB laser is only a few microns. In order to prevent the light directly reflected from the Si_3N_4 chip facet from interfering with the laser, the laser needs to be slightly tilted. The alignment stage where the DFB laser is actually placed has a six-axis drive that can achieve adjustment at any angle.

Once the laser is successfully coupled to the Si_3N_4 chip, the resonant frequency of the microring should be aligned with the laser frequency to achieve self-injection locking. There are three ways to achieve it: adjusting the drive current of the laser, adjusting the operating temperature of the laser, and adjusting the temperature of the microring. We use the last method most often because it does not change the laser output power, so we can determine if the two resonant wavelengths are aligned by monitoring the output power of the microring. Usually when the two wavelengths are aligned, the light will be coupled into the microring and the output power will drop. This step only requires coarse adjustment of the microring temperature.

According to Eq. 3.11, the round trip time of the laser-microring

coupling has an impact on the optical feedback. To achieve stable self-injection locking, it is also necessary to carefully adjust the phase shift between the laser and the microring. Based on the previous step, we sweep the temperature of the microring and monitor the resonance waveform displayed by the oscilloscope to determine whether the phase shift is appropriate, as shown in Fig. 3.7(b). When the phase shift is not appropriate, the resonance is very narrow and shallow. By adjusting the phase shift by the temperature of the connecting waveguide between the microring and the DFB laser, it can be seen that the shape of the output resonance is constantly changing [96,102]. As the phase shift is gradually optimized, the resonance will become wider and eventually take on a 'U' shape. The wide resonance or the flat resonance peak means that near the resonant wavelength, the DFB laser is locked to the microring, and the output wavelength of the system is controlled by the resonant frequency of the microring, which is consistent with the frequency pulling in the theoretical analysis in the previous section.

After optimizing the phase shift, stop scanning the microring temperature but finely tune the temperature to align the resonant frequency of the microring with the DFB laser again. When the output power reaches the lowest and then self-injection locking of the DFB laser is achieved.

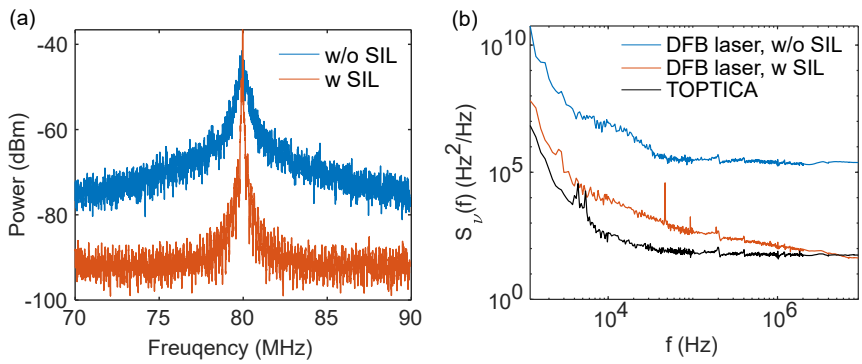

Figure 3.8: (a) Beating spectrum from self-heterodyne measurement. The frequency shift introduced by the AOM is 80 MHz. (b) Measured frequency noise PSDs of the DFB laser with and without self-injection locking, and a laser from TOPTICA.

As shown in Fig. 3.8(a), before self-injection locking, the linewidth of the beating spectrum is relatively wide, but once the DFB laser is locked to the microring with a Q factor of 15 million, the beating spectrum immediately becomes narrower. If we look at the frequency noise PSDs

shown in Fig. 3.8(b), when the DFB laser is free running, the intrinsic linewidth of the DFB laser is about 818 kHz. After self-injection locking, the intrinsic linewidth drops to 135 Hz, which is directly suppressed by more than 6000 times. Its intrinsic linewidth is comparable to or even a bit better than that of the commercial laser from TOPTICA (CTL 1550). However, higher thermal noise due to the small volume of the microring or the influence of environmental factors, the low-frequency noise of the laser is still a little worse. If compared with the lowest noise self-injection locked semiconductor lasers mentioned in Introduction [48], since the Q factor of our microring is lower than that of thin Si_3N_4 microrings, the intrinsic linewidth we obtained is still higher than theirs.

Chapter 4

Ultra-low loss silicon nitride waveguides

The previous chapters discussed in detail the intrinsic linewidth theory and how to suppress the intrinsic linewidth of a light source. We found that the reduction of the intrinsic linewidth depends strongly on the propagation loss of the passive platform and the size of the external cavity. Therefore, this chapter briefly introduces the waveguide losses, how to manufacture ultra-low loss waveguides in silicon nitride, and considerations for manufacturing long waveguides.

4.1 Waveguide losses

Taking the microring shown in the Fig. 4.1 as an example, there are four main sources of waveguide losses: absorption loss due to the material itself, bending loss introduced when the waveguide bending radius is small, scattering loss caused by sidewall and surface roughness or film defects, and radiation loss because of particles or other structures close to the waveguide [38, 103–106]. Of course, except the absorption loss that will be converted into heat dissipation, the other three losses usually convert the guided modes in the waveguide into unconfined modes and then dissipate. [38].

For Si_3N_4 films deposited using low-pressure chemical vapor deposition (LPCVD), high temperature annealing can break the N-H bonds and eliminate the absorption peak near the wavelength of 1520 nm [107, 108]. The bending loss can be reduced by increasing the bending radius. When manufacturing waveguides, extra attention should be paid to the clean-

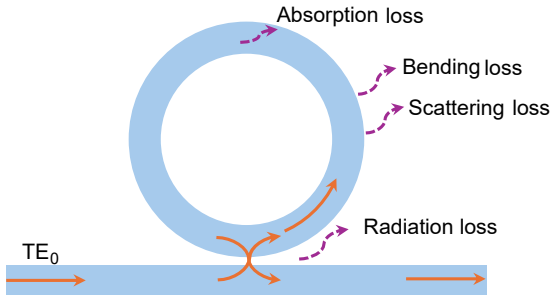

Figure 4.1: Schematic of waveguide losses. The orange solid arrows represent fundamental mode (TE_0) propagation, and the purple dashed arrows represent waveguide losses.

liness of the chip surface, otherwise there will be too many particles near the waveguides, which will greatly increase the radiation loss of the waveguides.

When designing devices, increase the spacing between unrelated waveguides to avoid potential coupling and radiation loss. If two waveguides need to be closely coupled, such as a microring and a bus waveguide, some special designs can be used to decrease the radiation loss. For example, a racetrack type microring is used to increase the coupling efficiency between the microring and the bus waveguide by extending the coupling waveguide length instead of reducing the gap width [36].

In addition, as shown in [Paper B], in order to improve the conversion efficiency and output power of OPOs, the gap between the bus waveguide and the microring needs to be as small as possible. The bus waveguide causes high radiation loss to the microring, but there is a Vernier effect between the fundamental mode and the higher-order mode in the microring, so that at certain specific wavelengths, the radiation loss of the microring waveguide will be reduced due to the bound state in the continuum effect [59]. Although the radiation loss resulted from the bus waveguide is reduced, the propagation loss of the microring waveguide is still limited by the sidewall or surface roughness.

The surface roughness of the waveguide can be reduced by optimizing the film deposition recipe or polishing [105], while the sidewall roughness is mainly reduced by optimizing the exposure and etching recipes, or using the method demonstrated in [Paper A], depositing an additional layer of very thin Si_3N_4 film after etching to smoothen the waveguide sidewall.

If the waveguide roughness cannot be optimized due to equipment

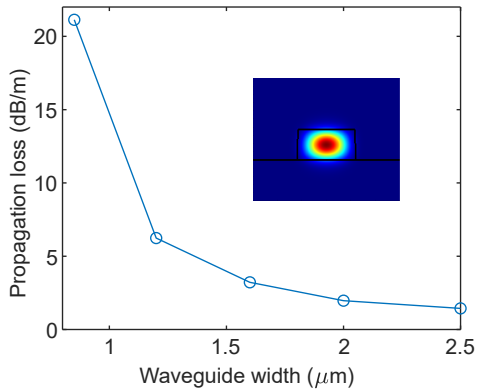

Figure 4.2: Relationship between propagation loss of the fundamental TE mode and waveguide width. The thickness of the Si_3N_4 waveguides is 740 nm. The test wavelength is from 1560 to 1620 nm, avoiding the absorption peak of LPCVD Si_3N_4. The measured propagation loss is the mean of statistical data of 36 samples measured at different wavelengths on the same chip.

limitations, the scattering loss caused by the waveguide roughness can also be reduced by increasing the waveguide size. As shown in Fig. 4.2, from 800 nm to 2.5 μm waveguide width, the propagation loss of the Si_3N_4 waveguides is reduced by more than ten times, and the lowest waveguide loss is close to 1.4 dB/m, since the fundamental TE mode is confined to the center of the waveguides. As the waveguide width increases, the optical field at the sidewall weakens, the effect of the sidewall roughness on the mode weakens, so the propagation loss caused by scattering decreases [109]. This method is simple and effective, so multimode waveguides are often used in low-loss applications.

4.2 Overview of process flow

The process flow for low-loss Si_3N_4 waveguides is shown in Fig. 4.3, where each step is crucial to achieve low loss performance. The process begins with the thermally oxidized 4-inch silicon wafers. Due to the high stress associated with thick Si_3N_4 films, crack barriers are essential to prevent cracking [110–112]. These barriers are created using photolithography and wet etching. The trench patterns are identical, allowing for the use of a mask aligner to expose the patterns. These patterns are then transferred into the thermal SiO_2 cladding through wet etching.

After standard cleaning to ensure a contaminant-free wafer surface,

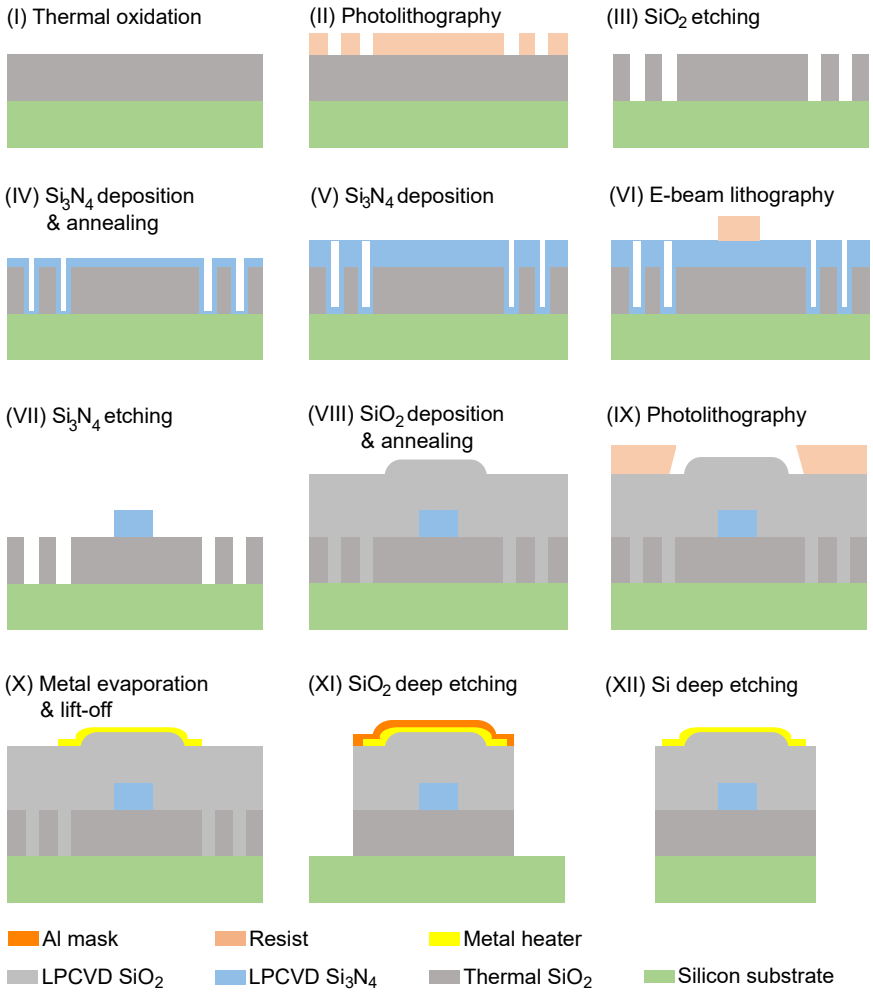

Figure 4.3: Process flow for low-loss thick Si_3N_4 waveguide with metal microheaters consisting of titanium and platinum on top. The Al mask in step XI is prepared in the same way as step IX and X.

Si_3N_4 is deposited on the SiO_2 cladding using LPCVD. Once the Si_3N_4 film reaches a thickness of approximately 400 nm, high-temperature annealing is performed to relieve the stress in the thick film and to break the N-H bonds formed during LPCVD [107, 108]. Following annealing, a second Si_3N_4 layer is deposited using the same deposition process.

The entire fabrication process follows a subtractive approach [108, 113]. Once the thick Si_3N_4 film is deposited, e-beam lithography and

dry etching are employed to define the desired waveguide patterns. Most of the Si_3N_4 film is removed during the dry etching process because it is not protected by the negative resist. Fig. 4.4(a) shows the etched Si_3N_4 waveguide, where the line roughness on the waveguide sidewall is clearly visible. After etching the Si_3N_4 waveguides, a second high-temperature annealing step is performed to further break the N-H bonds. Subsequently, approximately 3 μm of SiO_2 cladding is deposited layer by layer, with additional annealing steps to release stress and densify the films.

To improve tunability, microheaters are added to the wafer. The refractive index of Si_3N_4 can be controlled by temperature. As the temperature increases, the refractive index also increases. The microheaters are fabricated using photolithography and lift-off. Since several heaters often need to be controlled simultaneously in experiments, when designing the heater contact electrodes, different heaters share the same ground electrode, and different heaters are spaced as far as possible to avoid thermal crosstalk.

For coupling light from lensed fibers into the Si_3N_4 chips, edge couplers are used [114]. To release the chips from the wafer, dry etching is employed. The release trenches are defined by photolithography, and an aluminum (Al) film is evaporated to serve as a hard mask, improving etching selectivity [115, 116]. After the SiO_2 cladding is fully etched, we use another dry etching tool to perform the Si deep etching. Since that tool only allows the use of photoresist as a mask, a final photolithography step will once again define the trenches. Finally, the silicon substrate is almost completely etched to release the chips.

4.3 Considerations for manufacturing long waveguides

Whether it is a narrow-linewidth semiconductor laser with external cavity or the self-injection locking method, ultra-low propagation loss and a long feedback loop are both required. The previous section introduced how to manufacture low-loss Si_3N_4 waveguides or microrings. This section will introduce the matters that require extra attention when manufacturing low-loss long waveguides.

We use e-beam lithography to pattern Si_3N_4 waveguides. The writing field of e-beam exposure refers to the maximum field that the electron beam can be deflected to expose the resist without moving the sample.

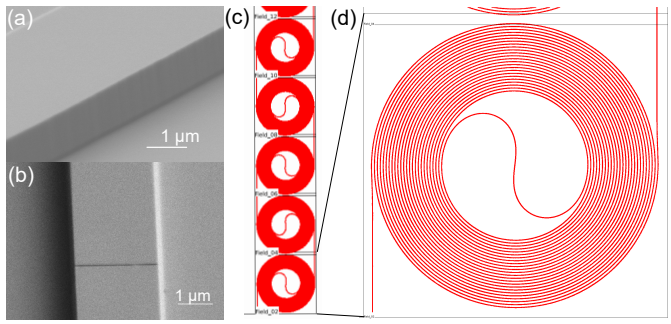

Figure 4.4: (a) SEM image of a Si_3N_4 waveguide. (b) SEM image of a long Si_3N_4 waveguide with stitching error at the interface of adjacent writing fields. (c) Arrangement of the writing fields for long waveguides. (d) A detailed writing field. The black box represents a writing field, and the red curve represents the waveguide.

The maximum writing field of the machine we use is 1040 μm × 1040 μm. Stitching errors may occur at the interface between adjacent writing fields, as shown in Fig. 4.4(b). When exposing across the writing field, the waveguide may break or be misaligned. These stitching errors may be as large as several hundred nanometers and cause extra scattering losses. Stitching errors are not mainly caused by the movement of the stage that holds the sample, because the stage position is precisely controlled by a laser interferometer. Stitching errors mainly come from imperfect deflection of the electron beam [41]. The chip height must be strictly checked before exposure to ensure that the chip surface is flat, which can effectively reduce stitching errors.

The size of the microring is generally smaller than this size, so the stitching errors at the interface of adjacent writing fields can be safely avoided. When preparing meter-long waveguides, the same waveguide inevitably spans multiple writing fields. In order to reduce the space occupied by the waveguides, improve the compactness, take into account the uniformity of the Si_3N_4 film thickness, and more importantly, avoid excessive cross writing field exposure, the long waveguide is designed as multiple cascaded spirals so that the long waveguide is distributed in a smaller area as much as possible.

Each spiral waveguide is arranged in one writing field, as shown in Fig. 4.4(c). The writing fields are exposed in sequence following the propagation direction of the waveguide. Since the multi-pass mode (2 times) is adopted [117], that is, the writing field is exposed twice accord-

ing to the same operation, so the number of write fields in the figure is even. The maximum diameter of the spiral waveguide does not exceed the size of the writing field, as shown in 4.4(d). Inside the writing field, the electron beam exposes the waveguide following the geometric shape along the propagation direction of the waveguide.

Chapter 5

Summary and future outlook

This thesis analyzes the frequency noise sources in semiconductor lasers and soliton microcombs, along with the theoretical predictions of their intrinsic linewidths. It also demonstrates how passive external cavities and self-injection locking technologies effectively suppress frequency noise. For the semiconductor laser noise suppression, a DFB laser is self-injection locked to a low-loss silicon nitride microring resonator to achieve an intrinsic linewidth of 135 Hz. Although this technology has been realized in recent years, it is the first time it has been demonstrated in our laboratory. Regarding the linewidth reduction for soliton microcombs, the intrinsic linewidth of the comb lines is reduced to below 1 Hz through the use of an external low-loss and long fiber loop. This method is novel and simple, and its performance is comparable to that of current narrow-linewidth soliton microcombs.

Future research can be carried out from the following aspects.

The first is the semiconductor laser self-injection locking to complex microresonator structures. So far, almost all reported work uses a semiconductor laser locked to a single microresonator. Would the dynamics and performance be different if coupled microresonators are used? This is a question worth studying.

Additionally, when the DFB laser is coupled to a low-loss silicon nitride chip and the self-injection locked regime is overlapped with the soliton generation regime by adjusting the laser's driving current, temperature, a microcomb with narrow linewidth can be directly pumped by the DFB laser. This configuration has good repeatability and is plug-and-play, which can avoid the tediousness of other soliton generation methods. If self-injection locking can be used to achieve narrow-linewidth,

high-efficiency soliton microcombs, it will be unprecedented.

The last is heterogeneous integrated soliton microcombs. Although heterogeneous integration is relatively mature as mentioned in Introduction, most of the researches are on thin silicon nitride platforms, and heterogeneous integration on dispersion-engineered silicon nitride platforms needs to be further improved. Based on the previous questions, if a fully on-chip narrow-linewidth and high-efficiency soliton microcomb can be realized, it will provide great help for future soliton applications.

Chapter 6

Summary of papers

Paper A

Low-loss dispersion-engineered silicon nitride waveguides coated with a thin blanket layer,
Conference on Lasers and Electro-Optics, San Jose, USA, paper JW3B.183, 2022.

In this work, we coated an 8 nm thick Si_3N_4 blanket layer on etched Si_3N_4 waveguides, and we found that the thin layer can effectively reduce the propagation loss in the highly confined Si_3N_4 waveguide, but does not affect the group velocity dispersion much.

My contributions: I simulated the mode and dispersion of Si_3N_4 waveguides, characterized the devices. I wrote the paper with support from the co-authors and presented the work at CLEO 2022.

Paper B

High-power on-chip hyperparametric oscillator,
to be submitted, 2024.

In this work, we numerically demonstrated strong coupling and high pump power can provide high output power for optical hyperparametric oscillators. Microring based on bound states in the continuum periodically exhibit high intrinsic Q factors to suppress mode competition, thereby achieving high-efficiency. After optimization, we experimentally

presented a high-power optical hyperparametric oscillator whose signal wave has an on-chip power of 215 mW and an intrinsic linewidth of 220 Hz.

My contributions: I did the simulation, fabricated and characterized the devices. I did the experiments. I wrote the manuscript with support from the co-authors.

Paper C

Self-injection-locked optical parametric oscillator based on microcombs,
Optica, vol. 11, no. 3, pp. 420-426, 2024.

In this work, we demonstrated a sub-Hz linewidth optical parametric oscillator through self-injection locking a single comb line from a soliton microcomb. We revealed a dynamics similar to that found in conventional lasers using self-injection locking and showed that there exists a dynamic regime where the frequency noise of the comb line can be consistently reduced to three orders of magnitude below the pump.

My contributions: I assisted with the experiments and paper writing, and performed a supplementary experiment.

References

[1] T. H. Maiman, R. Hoskins, I. d'Haenens, C. K. Asawa, and V. Evtuhov, "Stimulated optical emission in fluorescent solids. ii. spectroscopy and stimulated emission in ruby," *Physical Review*, vol. 123, no. 4, p. 1151, 1961.

[2] Q. Cheng, M. Bahadori, M. Glick, S. Rumley, and K. Bergman, "Recent advances in optical technologies for data centers: a review," *Optica*, vol. 5, no. 11, pp. 1354–1370, 2018.

[3] K. Gasmi, A. Aljalal, and W. Al-Basheer, "Blue external-cavity diode laser for no2 gas detection," in *Semiconductor Lasers and Laser Dynamics IX*, vol. 11356. SPIE, 2020, pp. 140–147.

[4] Q.-F. Yang, B. Shen, H. Wang, M. Tran, Z. Zhang, K. Y. Yang, L. Wu, C. Bao, J. Bowers, A. Yariv *et al.*, "Vernier spectrometer using counterpropagating soliton microcombs," *Science*, vol. 363, no. 6430, pp. 965–968, 2019.

[5] Y. Dai, T. Fu, J. Chen, C. Tang, X. Wang, Y. Wang, and W. Zheng, "High-power semiconductor laser with a narrow linewidth based on transverse photonic crystal," *Optics Express*, vol. 32, no. 20, pp. 36 010–36 020, 2024.

[6] H. Stoehr, F. Mensing, J. Helmcke, and U. Sterr, "Diode laser with 1 hz linewidth," *Optics letters*, vol. 31, no. 6, pp. 736–738, 2006.

[7] C. V. Poulton, M. J. Byrd, P. Russo, E. Timurdogan, M. Khandaker, D. Vermeulen, and M. R. Watts, "Long-range lidar and free-space data communication with high-performance optical phased arrays," *IEEE Journal of Selected Topics in Quantum Electronics*, vol. 25, no. 5, pp. 1–8, 2019.

[8] L. Krinner, K. Dietze, L. Pelzer, N. Spethmann, and P. Schmidt, "Low phase noise cavity transmission self-injection locked diode laser system for atomic physics experiments," *Optics Express*, vol. 32, no. 9, pp. 15 912–15 922, 2024.

[9] Q. Zhao, Z. Zhang, B. Wu, T. Tan, C. Yang, J. Gan, H. Cheng, Z. Feng, M. Peng, Z. Yang *et al.*, "Noise-sidebands-free and ultra-low-rin 1.5 μm single-frequency fiber laser towards coherent optical detection," *Photonics Research*, vol. 6, no. 4, pp. 326–331, 2018.

[10] Z. L. Newman, V. Maurice, T. Drake, J. R. Stone, T. C. Briles, D. T. Spencer, C. Fredrick, Q. Li, D. Westly, B. R. Ilic *et al.*, "Architecture for the photonic integration of an optical atomic clock," *Optica*, vol. 6, no. 5, pp. 680–685, 2019.

[11] Z. Bai, Z. Zhao, M. Tian, D. Jin, Y. Pang, S. Li, X. Yan, Y. Wang, and Z. Lu, "A comprehensive review on the development and applications of narrow-linewidth lasers," *Microwave and Optical Technology Letters*, vol. 64, no. 12, pp. 2244–2255, 2022.

[12] Y. Peng, X. Wei, G. Xie, J. Gao, D. Li, and W. Wang, "A high-power narrow-linewidth optical parametric oscillator based on pp-mgln," *Laser Physics*, vol. 23, no. 5, p. 055405, 2013.

[13] W. Wang, L. Wang, and W. Zhang, "Advances in soliton micro-comb generation," *Advanced Photonics*, vol. 2, no. 3, pp. 034 001–034 001, 2020.

[14] Z. Zhou, X. Ou, Y. Fang, E. Alkhazraji, R. Xu, Y. Wan, and J. E. Bowers, "Prospects and applications of on-chip lasers," *Elight*, vol. 3, no. 1, p. 1, 2023.

[15] W. Liang, V. Ilchenko, D. Eliyahu, A. Savchenkov, A. Matsko, D. Seidel, and L. Maleki, "Ultralow noise miniature external cavity semiconductor laser," *Nature communications*, vol. 6, no. 1, p. 7371, 2015.

[16] T. L. Koch and U. Koren, "Semiconductor lasers for coherent optical fiber communications," *Journal of lightwave technology*, vol. 8, no. 3, pp. 274–293, 1990.

[17] S. Selmic, S. L. Wilson, G. Evans, J. B. Kirk, Z. A. Alhilali, and D. Phan, "High-power single-frequency semiconductor lasers,"

in *2001 IEEE Emerging Technologies Symposium on BroadBand Communications for the Internet Era. Symposium Digest (Cat. No. 01EX508)*. IEEE, 2001, pp. 48–52.

[18] R. N. Hall, G. E. Fenner, J. Kingsley, T. Soltys, and R. Carlson, "Coherent light emission from gaas junctions," *Physical Review Letters*, vol. 9, no. 9, p. 366, 1962.

[19] C. Henry, "Theory of the linewidth of semiconductor lasers," *IEEE Journal of Quantum Electronics*, vol. 18, no. 2, pp. 259–264, 1982.

[20] S. Wang, "Principles of distributed feedback and distributed bragg-reflector lasers," *IEEE Journal of Quantum Electronics*, vol. 10, no. 4, pp. 413–427, 1974.

[21] H. Kogelnik and C. Shank, "Stimulated emission in a periodic structure," *Applied Physics Letters*, vol. 18, no. 4, pp. 152–154, 1971.

[22] Y. Yamamoto, S. Saito, and T. Mukai, "Am and fm quantum noise in semiconductor lasers-part ii: Comparison of theoretical and experimental results for algaas lasers," *IEEE Journal of Quantum Electronics*, vol. 19, no. 1, pp. 47–58, 1983.

[23] W. Streifer, R. Burnham, and D. Scifres, "Effect of external reflectors on longitudinal modes of distributed feedback lasers," *IEEE Journal of Quantum Electronics*, vol. 11, no. 4, pp. 154–161, 1975.

[24] S. Saito, O. Nilsson, and Y. Yamamoto, "Oscillation center frequency tuning, quantum fm noise, and direct frequency characteristics in external grating loaded semiconductor lasers," *IEEE Journal of Quantum Electronics*, vol. 18, no. 6, pp. 961–970, 1982.

[25] K. Choi, J. Menders, P. Searcy, and E. Korevaar, "Optical feedback locking of a diode laser using a cesium faraday filter," *Optics communications*, vol. 96, no. 4-6, pp. 240–244, 1993.

[26] X. Zhang, N. Wang, L. Gao, M. Feng, B. Chen, Y. H. Tsang, and A. Liu, "Narrow-linewidth external-cavity tunable lasers," in *10th International Conference on Optical Communications and Networks (ICOCN 2011)*. IET, 2011, pp. 1–2.

[27] D. J. Thompson and R. E. Scholten, "Narrow linewidth tunable external cavity diode laser using wide bandwidth filter," *Review of scientific instruments*, vol. 83, no. 2, 2012.

[28] E. Patzak, H. Olesen, A. Sugimura, S. Saito, and T. Mukai, "Spectral linewidth reduction in semiconductor lasers by an external cavity with weak optical feedback," *Electronics Letters*, vol. 22, no. 19, pp. 938–940, 1983.

[29] H. Li and N. Abraham, "Analysis of the noise spectra of a laser diode with optical feedback from a high-finesse resonator," *IEEE journal of quantum electronics*, vol. 25, no. 8, pp. 1782–1793, 1989.

[30] J. Lawrence and D. Kane, "Injection locking suppression of coherence collapse in a diode laser with optical feedback," *Optics communications*, vol. 167, no. 1-6, pp. 273–282, 1999.

[31] I. Breunig, D. Haertle, and K. Buse, "Continuous-wave optical parametric oscillators: recent developments and prospects," *Applied Physics B*, vol. 105, pp. 99–111, 2011.

[32] M. H. Dunn and M. Ebrahimzadeh, "Parametric generation of tunable light from continuous-wave to femtosecond pulses," *Science*, vol. 286, no. 5444, pp. 1513–1517, 1999.

[33] B. Jacobsson, M. Tiihonen, V. Pasiskevicius, and F. Laurell, "Narrowband bulk bragg grating optical parametric oscillator," *Optics letters*, vol. 30, no. 17, pp. 2281–2283, 2005.

[34] M. Vainio, C. Ozanam, V. Ulvila, and L. Halonen, "Tuning and stability of a singly resonant continuous-wave optical parametric oscillator close to degeneracy," *Optics Express*, vol. 19, no. 23, pp. 22 515–22 527, 2011.

[35] J. Saikawa, M. Fujii, H. Ishizuki, and T. Taira, "High-energy, narrow-bandwidth periodically poled mg-doped linbo 3 optical parametric oscillator with a volume bragg grating," *Optics letters*, vol. 32, no. 20, pp. 2996–2998, 2007.

[36] L. Zhang, S. Hong, Y. Wang, H. Yan, Y. Xie, T. Chen, M. Zhang, Z. Yu, Y. Shi, L. Liu *et al.*, "Ultralow-loss silicon photonics beyond the singlemode regime," *Laser & Photonics Reviews*, vol. 16, no. 4, p. 2100292, 2022.

[37] M. J. Heck, J. F. Bauters, M. L. Davenport, D. T. Spencer, and J. E. Bowers, "Ultra-low loss waveguide platform and its integration with silicon photonics," *Laser & Photonics Reviews*, vol. 8, no. 5, pp. 667–686, 2014.

[38] M. W. Puckett, K. Liu, N. Chauhan, Q. Zhao, N. Jin, H. Cheng, J. Wu, R. O. Behunin, P. T. Rakich, K. D. Nelson *et al.*, "422 million intrinsic quality factor planar integrated all-waveguide resonator with sub-mhz linewidth," *Nature communications*, vol. 12, no. 1, p. 934, 2021.

[39] X. Ji, F. A. Barbosa, S. P. Roberts, A. Dutt, J. Cardenas, Y. Okawachi, A. Bryant, A. L. Gaeta, and M. Lipson, "Ultra-low-loss on-chip resonators with sub-milliwatt parametric oscillation threshold," *Optica*, vol. 4, no. 6, pp. 619–624, 2017.

[40] D. T. Spencer, J. F. Bauters, M. J. Heck, and J. E. Bowers, "Integrated waveguide coupled si 3 n 4 resonators in the ultrahigh-q regime," *Optica*, vol. 1, no. 3, pp. 153–157, 2014.

[41] Z. Ye, "Ultralow-loss silicon nitride waveguides for nonlinear optics," Ph.D. dissertation, Chalmers Tekniska Hogskola (Sweden), 2021.

[42] R. J. Deri and E. Kapon, "Low-loss iii-v semiconductor optical waveguides," *IEEE Journal of Quantum Electronics*, vol. 27, no. 3, pp. 626–640, 1991.

[43] C. Ciminelli, D. D'Agostino, G. Carnicella, F. Dell'Olio, D. Conteduca, H. P. Ambrosius, M. K. Smit, and M. N. Armenise, "A high-q inp resonant angular velocity sensor for a monolithically integrated optical gyroscope," *IEEE Photonics Journal*, vol. 8, no. 1, pp. 1–19, 2015.

[44] M. Zhang, C. Wang, R. Cheng, A. Shams-Ansari, and M. Lončar, "Monolithic ultra-high-q lithium niobate microring resonator," *Optica*, vol. 4, no. 12, pp. 1536–1537, 2017.

[45] Y. Gao, F. Lei, M. Girardi, Z. Ye, R. Van Laer, V. Torres-Company, and J. Schröder, "Compact lithium niobate microring resonators in the ultrahigh q/v regime," *Optics Letters*, vol. 48, no. 15, pp. 3949–3952, 2023.

[46] Y. Fan, A. van Rees, P. J. Van der Slot, J. Mak, R. M. Oldenbeuving, M. Hoekman, D. Geskus, C. G. Roeloffzen, and K.-J. Boller, "Hybrid integrated inp-si 3 n 4 diode laser with a 40-hz intrinsic linewidth," *Optics express*, vol. 28, no. 15, pp. 21 713–21 728, 2020.

[47] Y. Fan, R. M. Oldenbeuving, E. J. Klein, C. J. Lee, H. Song, M. R. Khan, H. L. Offerhaus, P. J. van der Slot, and K.-J. Boller, "A hybrid semiconductor-glass waveguide laser," in *Laser Sources and Applications II*, vol. 9135. SPIE, 2014, pp. 231–236.

[48] B. Li, W. Jin, L. Wu, L. Chang, H. Wang, B. Shen, Z. Yuan, A. Feshali, M. Paniccia, K. J. Vahala *et al.*, "Reaching fiber-laser coherence in integrated photonics," *Optics Letters*, vol. 46, no. 20, pp. 5201–5204, 2021.

[49] M. A. Tran, D. Huang, J. Guo, T. Komljenovic, P. A. Morton, and J. E. Bowers, "Ring-resonator based widely-tunable narrow-linewidth si/inp integrated lasers," *IEEE Journal of Selected Topics in Quantum Electronics*, vol. 26, no. 2, pp. 1–14, 2019.

[50] C. Xiang, W. Jin, O. Terra, B. Dong, H. Wang, L. Wu, J. Guo, T. J. Morin, E. Hughes, J. Peters *et al.*, "3d integration enables ultralow-noise isolator-free lasers in silicon photonics," *Nature*, vol. 620, no. 7972, pp. 78–85, 2023.

[51] C. Xiang, W. Jin, J. Guo, J. D. Peters, M. Kennedy, J. Selvidge, P. A. Morton, and J. E. Bowers, "Narrow-linewidth iii-v/si/si 3 n 4 laser using multilayer heterogeneous integration," *Optica*, vol. 7, no. 1, pp. 20–21, 2020.

[52] K.-J. Boller, A. van Rees, Y. Fan, J. Mak, R. E. Lammerink, C. A. Franken, P. J. van der Slot, D. A. Marpaung, C. Fallnich, J. P. Epping *et al.*, "Hybrid integrated semiconductor lasers with silicon nitride feedback circuits," in *Photonics*, vol. 7, no. 1. Multidisciplinary Digital Publishing Institute, 2020, p. 4.

[53] W. Jin, Q.-F. Yang, L. Chang, B. Shen, H. Wang, M. A. Leal, L. Wu, M. Gao, A. Feshali, M. Paniccia *et al.*, "Hertz-linewidth semiconductor lasers using cmos-ready ultra-high-q microresonators," *Nature Photonics*, vol. 15, no. 5, pp. 346–353, 2021.

[54] C. Xiang, J. Liu, J. Guo, L. Chang, R. N. Wang, W. Weng, J. Peters, W. Xie, Z. Zhang, J. Riemensberger *et al.*, "Laser soliton microcombs heterogeneously integrated on silicon," *Science*, vol. 373, no. 6550, pp. 99–103, 2021.

[55] C. Xiang, W. Jin, and J. E. Bowers, "Silicon nitride passive and active photonic integrated circuits: trends and prospects," *Photonics Research*, vol. 10, no. 6, pp. A82–A96, 2022.

[56] E. Alkhazraji, W. W. Chow, F. Grillot, J. E. Bowers, and Y. Wan, "Linewidth narrowing in self-injection-locked on-chip lasers," *Light: Science & Applications*, vol. 12, no. 1, p. 162, 2023.

[57] C. Zhang, M. A. Tran, Z. Zhang, A. E. Dorche, Y. Shen, B. Shen, K. Asawa, G. Kim, N. Kim, F. Levinson *et al.*, "Integrated photonics beyond communications," *Applied Physics Letters*, vol. 123, no. 23, 2023.

[58] A. Malik, C. Xiang, L. Chang, W. Jin, J. Guo, M. Tran, and J. Bowers, "Low noise, tunable silicon photonic lasers," *Applied Physics Reviews*, vol. 8, no. 3, 2021.

[59] F. Lei, Z. Ye, K. Twayana, Y. Gao, M. Girardi, Ó. B. Helgason, P. Zhao, and V. Torres-Company, "Hyperparametric oscillation via bound states in the continuum," *Physical Review Letters*, vol. 130, no. 9, p. 093801, 2023.

[60] F. Riehle, *Frequency standards: basics and applications*. John Wiley & Sons, 2006.

[61] Z. Fang, H. Cai, G. Chen, and R. Qu, *Single frequency semiconductor lasers*. Springer, 2017.

[62] M. A. Tran, D. Huang, and J. E. Bowers, "Tutorial on narrow linewidth tunable semiconductor lasers using si/iii-v heterogeneous integration," *APL photonics*, vol. 4, no. 11, 2019.

[63] G. Di Domenico, S. Schilt, and P. Thomann, "Simple approach to the relation between laser frequency noise and laser line shape," *Applied optics*, vol. 49, no. 25, pp. 4801–4807, 2010.

[64] D. Elliott, R. Roy, and S. Smith, "Extracavity laser band-shape and bandwidth modification," *Physical Review A*, vol. 26, no. 1, p. 12, 1982.

[65] G. M. Stéphan, T. Tam, S. Blin, P. Besnard, and M. Têtu, "Laser line shape and spectral density of frequency noise," *Physical Review A—Atomic, Molecular, and Optical Physics*, vol. 71, no. 4, p. 043809, 2005.

[66] K. Kikuchi, "Impact of 1/f-type fm noise on coherent optical communications," *Electronics Letters*, vol. 17, no. 23, pp. 885–887, 1987.

[67] A. L. Schawlow and C. H. Townes, "Infrared and optical masers," *Physical review*, vol. 112, no. 6, p. 1940, 1958.

[68] J. Ohtsubo and J. Ohtsubo, *Semiconductor lasers and theory*. Springer, 2017.

[69] L. A. Coldren, S. W. Corzine, and M. L. Mashanovitch, *Diode lasers and photonic integrated circuits*. John Wiley & Sons, 2012, vol. 218.

[70] K. Vahala and A. Yariv, "Semiclassical theory of noise in semiconductor lasers-part i," *IEEE Journal of quantum electronics*, vol. 19, no. 6, pp. 1096–1101, 1983.

[71] C. Henry, "Theory of the phase noise and power spectrum of a single mode injection laser," *IEEE Journal of Quantum Electronics*, vol. 19, no. 9, pp. 1391–1397, 1983.

[72] C. Henry, "Phase noise in semiconductor lasers," *Journal of Lightwave Technology*, vol. 4, no. 3, pp. 298–311, 1986.

[73] K. Petermann, *Laser diode modulation and noise*. Springer Science & Business Media, 1991, vol. 3.

[74] H. Shu, L. Chang, Y. Tao, B. Shen, W. Xie, M. Jin, A. Netherton, Z. Tao, X. Zhang, R. Chen *et al.*, "Microcomb-driven silicon photonic systems," *Nature*, vol. 605, no. 7910, pp. 457–463, 2022.

[75] G. Moille, J. Stone, M. Chojnacky, R. Shrestha, U. A. Javid, C. Menyuk, and K. Srinivasan, "Kerr-induced synchronization of a cavity soliton to an optical reference," *Nature*, vol. 624, no. 7991, pp. 267–274, 2023.

[76] T. Herr, V. Brasch, J. D. Jost, C. Y. Wang, N. M. Kondratiev, M. L. Gorodetsky, and T. J. Kippenberg, "Temporal solitons in optical microresonators," *Nature Photonics*, vol. 8, no. 2, pp. 145–152, 2014.

[77] T. Herr, M. L. Gorodetsky, and T. J. Kippenberg, "Dissipative kerr solitons in optical microresonators," *Nonlinear optical cavity dynamics: from microresonators to fiber lasers*, pp. 129–162, 2016.

[78] O. Svelto, D. C. Hanna *et al.*, *Principles of lasers*. Springer, 2010, vol. 1.

[79] P. Liao, C. Bao, A. Kordts, M. Karpov, M. H. Pfeiffer, L. Zhang, A. Mohajerin-Ariaei, Y. Cao, A. Almaiman, M. Ziyadi *et al.*, "Dependence of a microresonator kerr frequency comb on the pump linewidth," *Optics Letters*, vol. 42, no. 4, pp. 779–782, 2017.

[80] M. Karpov, H. Guo, A. Kordts, V. Brasch, M. H. Pfeiffer, M. Zervas, M. Geiselmann, and T. J. Kippenberg, "Raman self-frequency shift of dissipative kerr solitons in an optical microresonator," *Physical review letters*, vol. 116, no. 10, p. 103902, 2016.

[81] Q.-F. Yang, X. Yi, K. Y. Yang, and K. Vahala, "Spatial-mode-interaction-induced dispersive waves and their active tuning in microresonators," *Optica*, vol. 3, no. 10, pp. 1132–1135, 2016.

[82] F. Lei, Z. Ye, Ó. B. Helgason, A. Fülöp, M. Girardi, and V. Torres-Company, "Optical linewidth of soliton microcombs," *Nature Communications*, vol. 13, no. 1, p. 3161, 2022.

[83] A. B. Matsko and L. Maleki, "On timing jitter of mode locked kerr frequency combs," *Optics express*, vol. 21, no. 23, pp. 28 862–28 876, 2013.

[84] C. Bao, M.-G. Suh, B. Shen, K. Şafak, A. Dai, H. Wang, L. Wu, Z. Yuan, Q.-F. Yang, A. B. Matsko *et al.*, "Quantum diffusion of microcavity solitons," *Nature Physics*, vol. 17, no. 4, pp. 462–466, 2021.

[85] J.-Q. Chen, C. Chen, J.-J. Sun, J.-W. Zhang, Z.-H. Liu, L. Qin, Y.-Q. Ning, and L.-J. Wang, "Linewidth measurement of a narrow-linewidth laser: Principles, methods, and systems," *Sensors*, vol. 24, no. 11, p. 3656, 2024.

[86] Z. Yuan, H. Wang, P. Liu, B. Li, B. Shen, M. Gao, L. Chang, W. Jin, A. Feshali, M. Paniccia *et al.*, "Correlated self-heterodyne method for ultra-low-noise laser linewidth measurements," *Optics Express*, vol. 30, no. 14, pp. 25 147–25 161, 2022.

[87] J. W. Dawson, N. Park, and K. J. Vahala, "An improved delayed self-heterodyne interferometer for linewidth measurements," *IEEE Photonics Technology Letters*, vol. 4, no. 9, pp. 1063–1066, 1992.

[88] Z. Zhao, Z. Bai, D. Jin, Y. Qi, J. Ding, B. Yan, Y. Wang, Z. Lu, and R. P. Mildren, "Narrow laser-linewidth measurement using short delay self-heterodyne interferometry," *Optics Express*, vol. 30, no. 17, pp. 30 600–30 610, 2022.

[89] E. Patzak, A. Sugimura, S. Saito, T. Mukai, and H. Olesen, "Semiconductor laser linewidth in optical feedback configurations," *Electronics letters*, vol. 19, no. 24, pp. 1026–1027, 1983.

[90] R. Kazarinov and C. Henry, "The relation of line narrowing and chirp reduction resulting from the coupling of a semiconductor laser to passive resonator," *IEEE Journal of quantum electronics*, vol. 23, no. 9, pp. 1401–1409, 1987.

[91] T. Komljenovic and J. E. Bowers, "Monolithically integrated high-q rings for narrow linewidth widely tunable lasers," *IEEE Journal of Quantum Electronics*, vol. 51, no. 11, pp. 1–10, 2015.

[92] K. Petermann, "External optical feedback phenomena in semiconductor lasers," *IEEE Journal of Selected Topics in Quantum Electronics*, vol. 1, no. 2, pp. 480–489, 1995.

[93] N. Schunk and K. Petermann, "Numerical analysis of the feedback regimes for a single-mode semiconductor laser with external feedback," *IEEE Journal of Quantum Electronics*, vol. 24, no. 7, pp. 1242–1247, 1988.

[94] K. Kikuchi and T. Okoshi, "Simple formula giving spectrum-narrowing ratio of semiconductor-laser output obtained by optical feedback," *Electronics Letters*, vol. 18, no. 1, pp. 10–12, 1982.

[95] P. Laurent, A. Clairon, and C. Breant, "Frequency noise analysis of optically self-locked diode lasers," *IEEE Journal of Quantum Electronics*, vol. 25, no. 6, pp. 1131–1142, 1989.

[96] N. Kondratiev, V. Lobanov, A. Cherenkov, A. Voloshin, N. Pavlov, S. Koptyaev, and M. Gorodetsky, "Self-injection locking of a laser diode to a high-q wgm microresonator," *Optics Express*, vol. 25, no. 23, pp. 28 167–28 178, 2017.

[97] A. Li, T. Van Vaerenbergh, P. De Heyn, P. Bienstman, and W. Bogaerts, "Backscattering in silicon microring resonators: a quantitative analysis," *Laser & Photonics Reviews*, vol. 10, no. 3, pp. 420–431, 2016.

[98] R. R. Galiev, N. M. Kondratiev, V. E. Lobanov, A. B. Matsko, and I. A. Bilenko, "Optimization of laser stabilization via self-injection locking to a whispering-gallery-mode microresonator," *Physical Review Applied*, vol. 14, no. 1, p. 014036, 2020.

[99] A. E. Shitikov, I. I. Lykov, O. V. Benderov, D. A. Chermoshentsev, I. K. Gorelov, A. N. Danilin, R. R. Galiev, N. M. Kondratiev, S. J. Cordette, A. V. Rodin *et al.*, "Optimization of laser stabilization via self-injection locking to a whispering-gallery-mode microresonator: experimental study," *Optics Express*, vol. 31, no. 1, pp. 313–327, 2022.

[100] B. Stern, X. Ji, A. Dutt, and M. Lipson, "Compact narrow-linewidth integrated laser based on a low-loss silicon nitride ring resonator," *Optics letters*, vol. 42, no. 21, pp. 4541–4544, 2017.

[101] B. Shen, X. Zhang, Y. Wang, Z. Tao, H. Shu, H. Chang, W. Li, Y. Zhou, Z. Ge, R. Chen *et al.*, "Reliable intracavity reflection for self-injection locking lasers and microcomb generation," *Photonics Research*, vol. 12, no. 5, pp. A41–A50, 2024.

[102] N. M. Kondratiev, V. E. Lobanov, A. E. Shitikov, R. R. Galiev, D. A. Chermoshentsev, N. Y. Dmitriev, A. N. Danilin, E. A. Lonshakov, K. N. Min'kov, D. M. Sokol *et al.*, "Recent advances in laser self-injection locking to high-q microresonators," *Frontiers of Physics*, vol. 18, no. 2, p. 21305, 2023.

[103] M. Gao, Q.-F. Yang, Q.-X. Ji, H. Wang, L. Wu, B. Shen, J. Liu, G. Huang, L. Chang, W. Xie *et al.*, "Probing material absorption and optical nonlinearity of integrated photonic materials," *Nature communications*, vol. 13, no. 1, p. 3323, 2022.

[104] A. Gondarenko, J. S. Levy, and M. Lipson, "High confinement micron-scale silicon nitride high q ring resonator," *Optics express*, vol. 17, no. 14, pp. 11 366–11 370, 2009.

[105] M. H. Pfeiffer, J. Liu, A. S. Raja, T. Morais, B. Ghadiani, and T. J. Kippenberg, "Ultra-smooth silicon nitride waveguides based

on the damascene reflow process: fabrication and loss origins," *Optica*, vol. 5, no. 7, pp. 884–892, 2018.

[106] X. Ji, S. Roberts, M. Corato-Zanarella, and M. Lipson, "Methods to achieve ultra-high quality factor silicon nitride resonators," *APL Photonics*, vol. 6, no. 7, 2021.

[107] K. N. Andersen, W. E. Svendsen, T. Stimpel-Lindner, T. Sulima, and H. Baumgärtner, "Annealing and deposition effects of the chemical composition of silicon-rich nitride," *Applied surface science*, vol. 243, no. 1-4, pp. 401–408, 2005.

[108] Z. Ye, A. Fülöp, Ó. B. Helgason, P. A. Andrekson, and V. Torres-Company, "Low-loss high-q silicon-rich silicon nitride microresonators for kerr nonlinear optics," *Optics letters*, vol. 44, no. 13, pp. 3326–3329, 2019.

[109] X. Ji, J. K. Jang, U. D. Dave, M. Corato-Zanarella, C. Joshi, A. L. Gaeta, and M. Lipson, "Exploiting ultralow loss multimode waveguides for broadband frequency combs," *Laser & Photonics Reviews*, vol. 15, no. 1, p. 2000353, 2021.

[110] C. Yang and J. Pham, "Characteristic study of silicon nitride films deposited by lpcvd and pecvd," *Silicon*, vol. 10, no. 6, pp. 2561–2567, 2018.

[111] C. G. Roeloffzen, M. Hoekman, E. J. Klein, L. S. Wevers, R. B. Timens, D. Marchenko, D. Geskus, R. Dekker, A. Alippi, R. Grootjans *et al.*, "Low-loss si3n4 triplex optical waveguides: Technology and applications overview," *IEEE journal of selected topics in quantum electronics*, vol. 24, no. 4, pp. 1–21, 2018.

[112] K. H. Nam, I. H. Park, and S. H. Ko, "Patterning by controlled cracking," *Nature*, vol. 485, no. 7397, pp. 221–224, 2012.

[113] Z. Ye, K. Twayana, P. A. Andrekson, and V. Torres-Company, "High-q si3n4 microresonators based on a subtractive processing for kerr nonlinear optics," *Optics express*, vol. 27, no. 24, pp. 35 719–35 727, 2019.

[114] X. Zhang, Y. Liang, Y. Chen, B. Shen, J. Huang, C. Lao, Y. Wu, Z. Li, D. Liu, H. Shu *et al.*, "300-nm-thick, ultralow-loss silicon nitride photonic integrated circuits by 8-in. foundry production," *Applied Physics Letters*, vol. 125, no. 12, 2024.

[115] B. Kim, K.-H. Kwon, and S.-H. Park, "Characterizing metal-masked silica etch process in a chf 3/cf 4 inductively coupled plasma," *Journal of Vacuum Science & Technology A: Vacuum, Surfaces, and Films*, vol. 17, no. 5, pp. 2593–2597, 1999.

[116] W.-T. Li, D. Bulla, and R. Boswell, "Surface oxidation of al masks for deep dry-etch of silica optical waveguides," *Surface and Coatings Technology*, vol. 201, no. 9-11, pp. 4979–4983, 2007.

[117] Z. Ye, F. Lei, K. Twayana, M. Girardi, P. A. Andrekson, and V. Torres-Company, "Integrated, ultra-compact high-q silicon nitride microresonators for low-repetition-rate soliton microcombs," *Laser & Photonics Reviews*, vol. 16, no. 3, p. 2100147, 2022.